Differential Regulation of Clathrin and Its Adaptor Proteins during Membrane Recruitment for Endocytosis[1][OPEN]

Chao Wang[2], Tianwei Hu[2], Xu Yan[2], Tingting Meng, Yutong Wang, Qingmei Wang, Xiaoyue Zhang, Ying Gu, Clara Sánchez-Rodríguez, Astrid Gadeyne, Jinxing Lin, Staffan Persson, Daniël Van Damme, Chuanyou Li, Sebastian Y. Bednarek, and Jianwei Pan*

College of Chemistry and Life Sciences, Zhejiang Normal University, Jinhua 321004, China (C.W., T.H., X.Y., T.M., Y.W., Q.W., J.P.); State Key Laboratory of Plant Genomics, Institute of Genetics and Developmental Biology, Chinese Academy of Sciences, Beijing 100101, China (X.Z., C.L.); Department of Biochemistry and Molecular Biology, Pennsylvania State University, University Park, Pennsylvania 16802 (Y.G.); Department of Biology, Institute of Agricultural Sciences, Eidgenössisch Technische Hochschule Zurich, 8092 Zurich, Switzerland (C.S.-R.); Department of Plant Systems Biology, Vlaams Instituut voor Biotechnologie, Department of Plant Biotechnology and Bioinformatics, Ghent University, B–9052 Ghent, Belgium (A.G., D.V.D.); College of Biological Sciences and Biotechnology, Beijing Forestry University, Beijing 100083, China (J.L.); Australian Research Council Centre of Excellence in Plant Cell Walls, School of Biosciences, University of Melbourne, Parkville, Victoria 3010, Australia (S.P.); and Department of Biochemistry, University of Wisconsin, Madison, Wisconsin 53706 (S.Y.B.)

ORCID IDs: 0000-0002-6377-5132 (S.P.); 0000-0002-9385-4851 (D.V.D.); 0000-0003-0202-3890 (C.L.); 0000-0001-7465-1787 (S.Y.B.); 0000-0001-5155-4933 (J.P.).

In plants, clathrin-mediated endocytosis (CME) is dependent on the function of clathrin and its accessory heterooligomeric adaptor protein complexes, ADAPTOR PROTEIN2 (AP-2) and the TPLATE complex (TPC), and is negatively regulated by the hormones auxin and salicylic acid (SA). The details for how clathrin and its adaptor complexes are recruited to the plasma membrane (PM) to regulate CME, however, are poorly understood. We found that SA and the pharmacological CME inhibitor tyrphostin A23 reduce the membrane association of clathrin and AP-2, but not that of the TPC, whereas auxin solely affected clathrin membrane association, in Arabidopsis (*Arabidopsis thaliana*). Genetic and pharmacological experiments revealed that loss of AP2μ or AP2σ partially affected the membrane association of other AP-2 subunits and that the AP-2 subunit AP2σ, but not AP2μ, was required for SA- and tyrphostin A23-dependent inhibition of CME. Furthermore, we show that although AP-2 and the TPC are both required for the PM recruitment of clathrin in wild-type cells, the TPC is necessary for clathrin PM association in AP-2-deficient cells. These results indicate that developmental signals may differentially modulate the membrane recruitment of clathrin and its core accessory complexes to regulate the process of CME in plant cells.

Clathrin-mediated endocytosis (CME) is the predominant mode of membrane protein internalization from the plasma membrane (PM) in eukaryotic cells (Bitsikas et al., 2014; Kirchhausen et al., 2014). In plants, CME is essential for many developmental processes, nutrient uptake, and responses to biotic and abiotic stresses or stimuli (Chen et al., 2011; Baisa et al., 2013; Fan et al., 2015; Zhang et al., 2015). In addition to their role in the internalization of PM proteins and associated ligands, distinct clathrin-coated vesicles (CCVs) form at the trans-Golgi network/early endosome (TGN/EE), where the trafficking pathways involved in the transport of newly synthesized proteins to the PM or vacuole, and the delivery of endocytosed proteins from the PM, converge (Song et al., 2006; Viotti et al., 2010; Dettmer and Friml, 2011; Zouhar and Sauer, 2014). The formation of distinct CCVs at the PM and TGN/EE requires the recruitment of clathrin and organelle-specific adaptor protein complexes that aid in the temporal and spatial regulation of coated vesicle formation (Holstein, 2002; Lam et al., 2007a, 2007b; Hwang and Robinson, 2009).

Similar to the formation of CCVs in mammalian cells, the plant CCV core proteins include clathrin heavy chains (CHCs; Kitakura et al., 2011) and clathrin light chains (CLCs; Wang et al., 2013a; Yu, et al., 2016) as well as the evolutionarily conserved heterotetrameric adaptor protein (AP) complexes AP-1 (Park et al., 2013; Teh et al., 2013; Wang et al., 2013b) and AP-2 (Bashline et al., 2013; Di Rubbo et al., 2013; Fan et al., 2013; Kim et al., 2013; Yamaoka et al., 2013) that connect clathrin and membrane-associated lipids and/or cargo proteins at sites of CCV formation on the TGN/EE and PM, respectively. Although the AP-2 complex has been generally thought to function as a heterotetramer, consisting of two large (α/A and β/B), one medium (μ/M), and one small (σ/S) subunit(s), recent studies in *Caenorhabditis elegans* have indicated that AP-2 may

function as two partially independent α-σ and μ-β hemicomplexes (Gu et al., 2013).

In addition to the AP-2 complex, CCV formation at the PM in plant cells is dependent on the heterooctameric TPLATE complex (TPC; Gadeyne et al., 2014). The TPC is postulated to function during the early steps of CCV formation at the PM for the recruitment of clathrin and AP-2, as down-regulation of the TPC subunits TPLATE muniscin-like (TML) and TPLATE effectively blocks CME and also leads to a reduction of AP2α recruitment to the PM (Gadeyne et al., 2014). Evolutionarily, the TPC appears to predate the functional specification of the AP complexes, and homologs of the complex components are found in a range of eukaryotes, including *Dictyostelium* spp., with the notable exception of yeast and metazoans (Gadeyne et al., 2014; Hirst et al., 2014; Zhang et al., 2015). However, whereas the hexameric *Dictyostelium* spp. TPC-related complex, TPLATE SET (Hirst et al., 2014), is dispensable for growth and endocytosis, Arabidopsis (*Arabidopsis thaliana*) TPC subunit mutants display severe defects in plant growth and development and are strongly impaired in CME (Van Damme et al., 2006; Gadeyne et al., 2014).

In plant cells, CME is regulated by the plant hormones auxin and salicylic acid (SA), which rapidly inhibit CME and thereby affect the distribution of PM proteins, including the PIN-FORMED (PIN) auxin efflux transporters and the water channel protein PLASMA MEMBRANE INTRINSIC PROTEIN2A (PIP2A; Paciorek et al., 2005; Pan et al., 2009; Robert et al., 2010; Du et al., 2013; Wang et al., 2013a). The regulation of CME by auxin and SA occurs in a transcription-independent manner (Robert et al., 2010; Xu et al., 2010; Du et al., 2013). However, the details underlying how these two CME effectors modulate the activity of core and accessory proteins required for CCV formation remain to be defined.

The phosphotyrosine analog tyrphostin A23 (TyrA23) has been utilized as a pharmacological tool to interfere with CME in animal and plant cells. In animal cells, TyrA23 is thought to impair the interactions between the AP2μ subunit and cargo proteins, leading to general inhibition of CME (Crump et al., 1998; Banbury et al., 2003). Likewise in plants, TyrA23 disrupts the PM association of AP2α1 (Di Rubbo et al., 2013; Kim et al., 2013), AP2μ (Yamaoka et al., 2013), AP2σ (Fan et al., 2013), and the TPC subunit TPLATE (Van Damme et al., 2011) and inhibits the internalization of a number of PM-resident proteins involved in hormone signaling (Robert et al., 2010; Irani et al., 2012), nutrient uptake (Barberon et al., 2011), and pathogen defense or stress response (Beck et al., 2012; Hao et al., 2014; Smith et al., 2014a, 2014b).

In this study, we examined the PM recruitment of clathrin as well as the AP-2 complex and TPC during CME in plant cells. Our results indicate that clathrin recruitment to the PM is dependent on the functions of the AP-2 complex and TPC and that the membrane recruitment of clathrin and its core accessory complexes is differentially regulated by the plant hormones auxin and SA and the pharmacological agent TyrA23.

RESULTS

Auxin and SA Modulate the Membrane Association of CHCs and CLCs Differentially

CLCs and CHCs assemble to form clathrin triskelia in vivo (McMahon and Boucrot, 2011; Kirchhausen, 2012). Despite the association of CLCs with CHCs, we have shown previously that the initial loss of membrane-associated CLC1 is paradoxically accompanied by a transient increase of membrane-associated CHCs after 5 to 30 min of treatment in auxin-treated plant cells (Wang et al., 2013a). To validate that changes in the levels of endogenous auxin similarly affect CLC1 and CHC membrane association, we analyzed their subcellular distribution in *WOX5:IAAH* transgenic lines (Blilou et al., 2005), which express the enzyme indoleacetamide hydrolase (IAAH) in the quiescent center of the root tip, by immunofluorescence (IF) microscopy using affinity-purified anti-CLC1 and anti-CHC antibodies. IAAH catalyzes the formation of indole-3-acetic acid (IAA) from the substrate, indole-3-acetamide (IAM), and previous studies in *WOX5:IAAH* lines have shown that application of IAM results in increased levels of auxin in the root columella, lateral root cap, and root epidermis (Blilou et al., 2005) as well as an inhibition of PIN2 endocytosis in root epidermal cells (Pan et al., 2009). Using similar conditions, we found that 5 μM IAM effectively induced the membrane dissociation of CLC1 and subsequently enhanced the membrane association of CHCs in the epidermal cells of the *WOX5:IAAH* roots but not in those of wild-type roots (Supplemental Fig. S1), confirming the differential auxin regulation of CLC and CHC recruitment to the membranes. Next, we examined the effect of changes in the distribution of endogenous auxin on the levels of membrane-associated CLC1 in epidermal cells of gravistimulated roots, in which an auxin gradient is generated upon gravity perception across the root cap with an accumulation on the new bottom side of the root (Paciorek, et al., 2005). Following a 2-h gravistimulation, the levels of membrane-associated CLC1 at the bottom side of the roots were reduced relative to those at the top side, but not in vertically grown roots (Fig. 1).

[1] This work was supported by the National Natural Science Foundation of China (grant nos. 91317304, 31370313, and 31171520), by a Vilas Associate Award from the University of Wisconsin, Madison, Graduate School (to S.Y.B.), and by the National Science Foundation (grant no. 1121998 to S.Y.B.).

[2] These authors contributed equally to the article.

* Address correspondence to jwpan@zjnu.cn.

The author responsible for distribution of materials integral to the findings presented in this article in accordance with the policy described in the Instructions for Authors (www.plantphysiol.org) is: Jianwei Pan (jwpan@zjnu.cn).

C.W., Y.G., A.G., S.P., J.L., D.V.D., C.L., S.Y.B., and J.P. designed research; C.W., T.H., X.Y., T.M., Y.W., Q.W., and X.Z. performed experiments; C.W., T.H., X.Y., T.M., Y.W., Q.W., S.P., J.L., D.V.D., C.L., S.Y.B., and J.P. analyzed the data; J.P. wrote the article; C.S.-R., S.P., D.V.D., S.Y.B., and J.P. revised the article.

[OPEN] Articles can be viewed without a subscription.

www.plantphysiol.org/cgi/doi/10.1104/pp.15.01716

Furthermore, statistical analysis (Supplemental Table S1) revealed that approximately 95% of the vertically grown roots had similar levels of membrane-associated CLC1 at both sides. By contrast, approximately 50% of the gravistimulated roots displayed a 20% reduction of CLC1 at the bottom side, indicating that the distribution and levels of endogenous auxin regulate clathrin membrane association in a physiologically relevant manner.

SA, which activates plant defense responses to a variety of biotic and abiotic stresses (Vlot et al., 2009; Rivas-San Vicente and Plasencia, 2011), inhibits CME and affects CLC2 association with the PM but not with the intracellular compartments (presumably TGN/EE; Du et al., 2013). To further examine the kinetic effects of SA on clathrin membrane association, we analyzed the subcellular localization of endogenous CLC1 and CHCs, and CLC1-GFP (driven by the 35S promoter), by IF microscopy and live-cell imaging, respectively, on wild-type root epidermal cells following time-course treatments with SA. Different from the previously observed effects of exogenous SA treatment (50 μM and 120 min; Du et al., 2013), lower concentrations of SA (25 μM) rapidly inhibited both the PM and intracellular compartment association of CLC1 (Fig. 2, A–D) and CLC1-GFP (Supplemental Fig. S2) within 5 to 30 min and enhanced PM- and intracellular compartment-associated

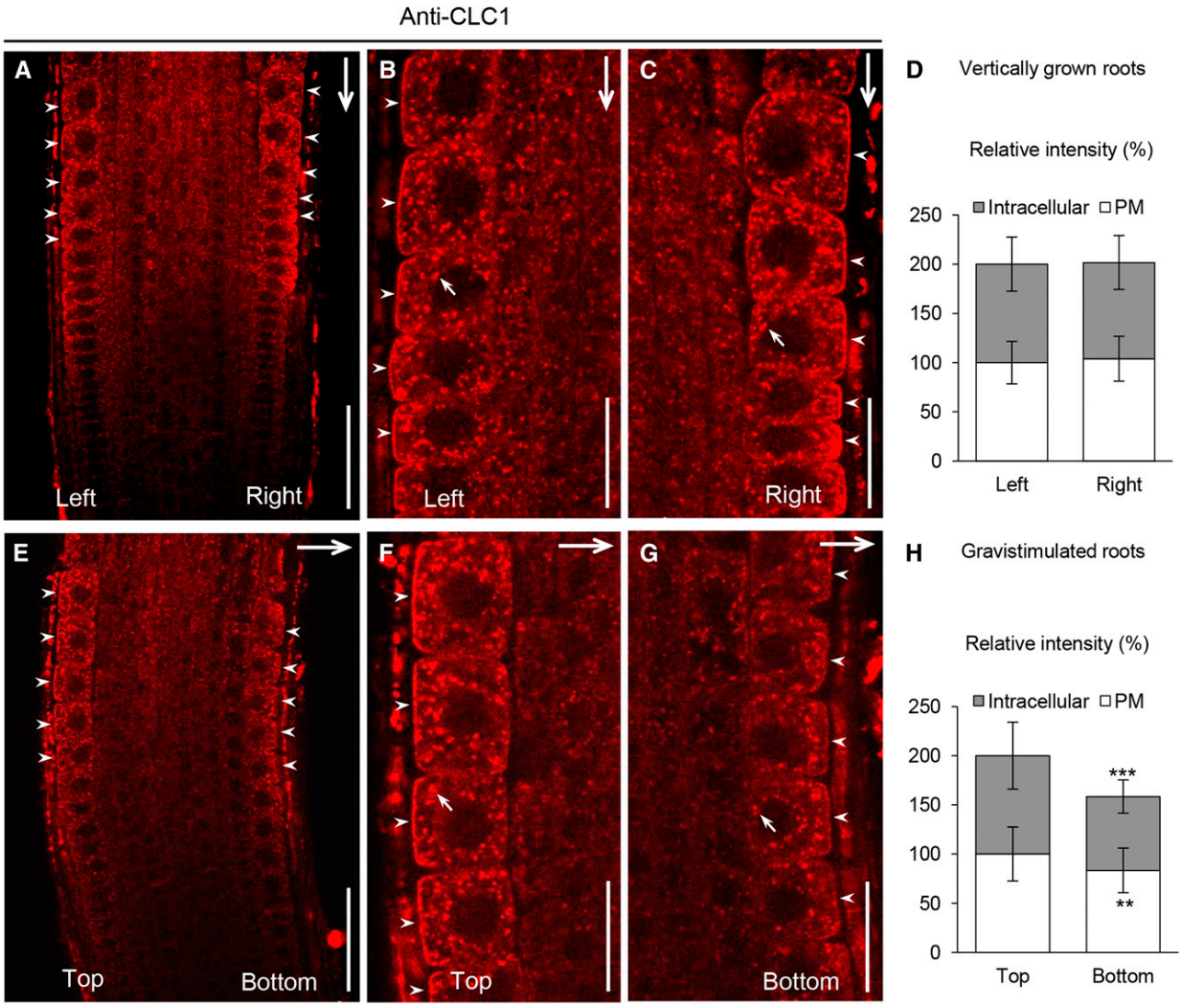

Figure 1. Effect of a gravity-induced auxin gradient on clathrin membrane association. A to D, Subcellular distribution of membrane-associated CLC1 at the left and right sides of vertically grown roots. E to H, Subcellular distribution of membrane-associated CLC1 at the top and bottom sides of 2-h gravistimulated roots. D and H show the relative intensity of membrane-associated CLC1 at both sides (B and C, $n = 37$; F and G, $n = 43$). The frequency distribution of ratios of both sides of individual roots is summarized in Supplemental Table S1. B, C, F, and G show higher magnification images of both sides of the roots shown in A and E. Arrows show the gravity vector or intracellular compartment-associated CLC1, while arrowheads show PM-associated CLC1 at both sides of the root. Values shown are means ± SD. **, $P < 0.01$ and ***, $P < 0.0001$ (Student's t test). Bars = 50 μm in A and E and 20 μm in B, C, F, and G.

levels of CHCs after 30 min (Fig. 2, K–N). Furthermore, the kinetic effects of SA on clathrin membrane association were different from those of the natural auxin IAA (Wang et al., 2013a) and the auxin analog 2,4-dichlorophenoxyacetic acid (2,4-D; Supplemental Fig. S3). In the presence of 2,4-D (10 μM), PM- and intracellular compartment-associated levels of CLC1 displayed transient loss and subsequent recovery to basal levels after 120 min, while the membrane-associated CHC levels showed an initial increase and a subsequent loss within 120 min (Supplemental Fig. S3). By contrast, in the presence of exogenous SA, the restoration of wild-type levels of membrane-associated CLC1 and CLC1-GFP was delayed significantly (240 min; Fig. 2, E–J; Supplemental Fig. S2), while the elevated levels of membrane-associated CHCs lasted longer (180 min; Fig. 2, O–T), compared with those in auxin-treated cells (60 min; Supplemental Fig. S3).

We corroborated these results by immunoblot analysis of microsomal membrane fractions from whole wild-type seedlings. Although no changes in the levels of membrane-associated CLC1/2 and CHC were detected in seedlings treated with 25 μM SA, application of 50 and 100 μM SA resulted in the reduction and elevation of microsome-associated CLC1/2 and CHC levels, respectively, 30 min after treatment (Supplemental Fig. S4A). The observed difference in the amount of SA required to interfere with the PM association of clathrin in roots (25 μM; Fig. 2) versus whole seedling microsomal membranes (50 or 100 μM; Supplemental Fig. S4A) may reflect cell and/or tissue-specific differences in the response to exogenous SA. Consistent with this, SA (25 μM) did not

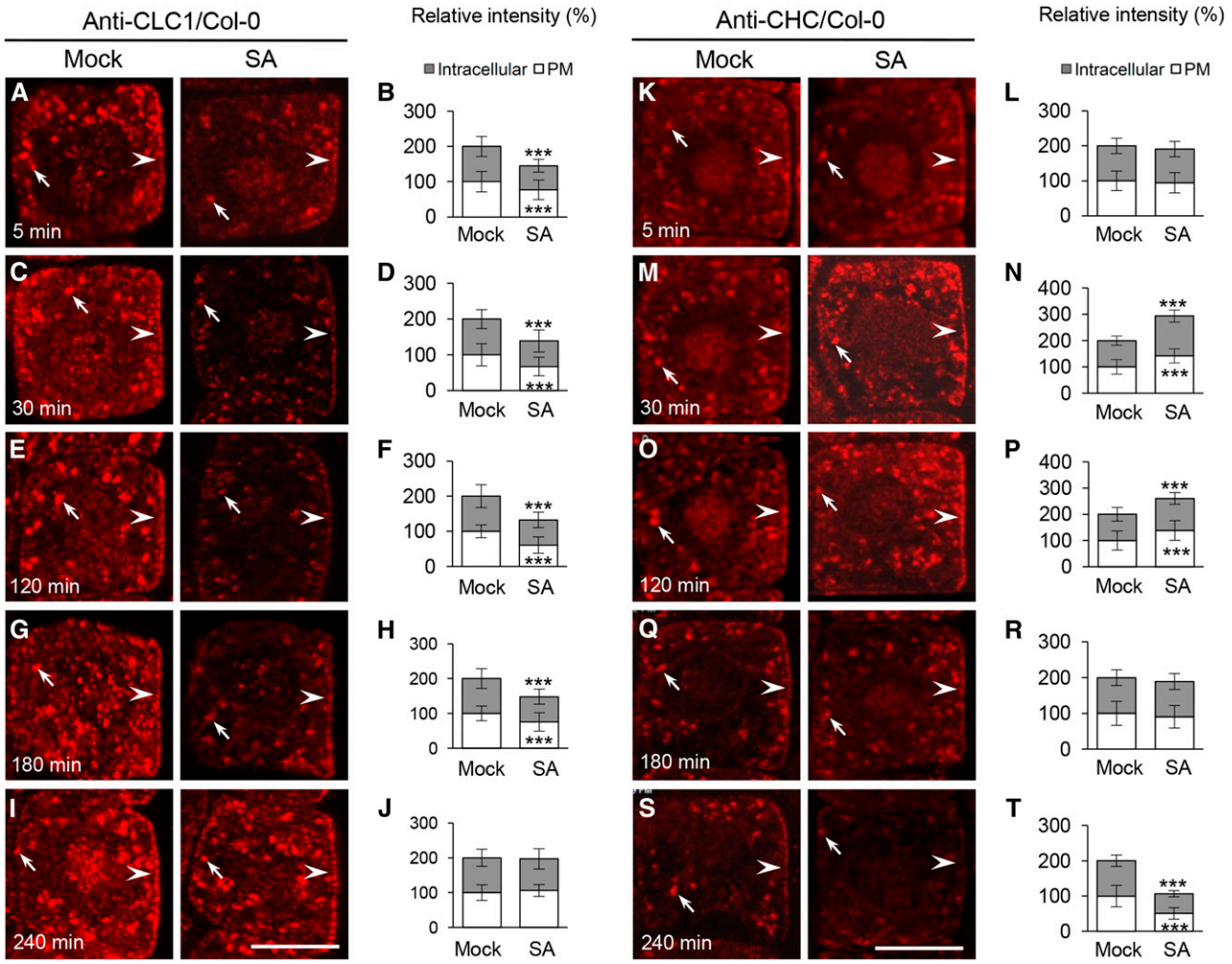

Figure 2. Kinetic effects of SA on clathrin membrane association. A to J, SA effects on membrane-associated CLC1 in the wild type. K to T, SA effects on membrane-associated CHC in the wild type. B, D, F, H, and J show the relative intensity of CLC1 at the PM and intracellular compartments (n = 66–105 cells from eight roots each). L, N, P, R, and T show the relative intensity of CHC at the PM and intracellular compartments (n = 62–86 cells from eight roots each). Different time lengths (5, 30, 120, 180, and 240 min) in mock (dimethyl sulfoxide [DMSO]) and SA (25 μM) treatments are indicated in the bottom left corners. Mock and SA treatments and antibodies are shown at the top. Arrows and arrowheads show intracellular compartment- and PM-associated CLC1 and CHC, respectively. Values shown are means ± SD. ***, $P < 0.0001$ (Student's t test). Bars = 10 μm.

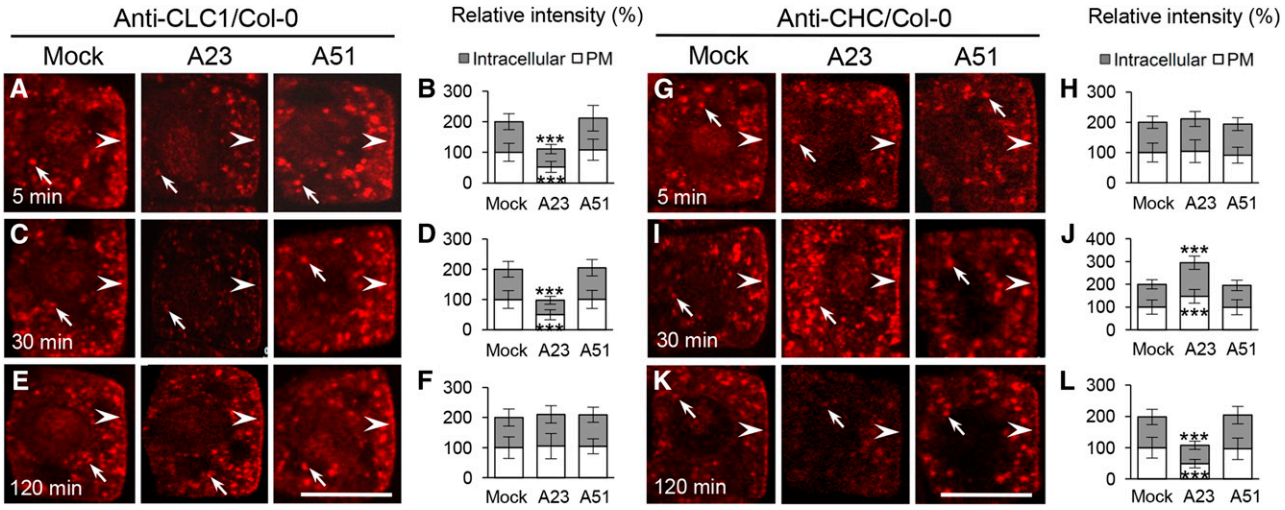

Figure 3. Kinetic effects of TyrA23 on clathrin membrane association. A to F, IF analysis of the TyrA23 effect on membrane-associated CLC1 in the wild type. G to L, IF analysis of the TyrA23 effect on membrane-associated CHC in the wild type. B, D, and F show the relative intensity of CLC1 at the PM and intracellular compartments (n = 62–98 cells from eight roots each). H, J, and L show the relative intensity of CHC at the PM and intracellular compartments (n = 60–95 cells from eight roots each). Treatments with DMSO (Mock), TyrA23 (A23; 30 μM), and TyrA51 (A51 [as a negative control]; 30 μM) are indicated at the top, whereas treatment time lengths (5, 30, and 120 min) are shown in the bottom left corners. Arrows and arrowheads show intracellular compartments and PM-associated CLC1 and CHC, respectively. Values shown are means ± SD. ***, $P < 0.0001$ (Student's t test; compared with the mock control). Bars = 10 μm.

affect the PM signals of CLC1/2-GFP in cotyledon epidermal cells (Supplemental Fig. S4B), indicating a lower sensitivity to, or uptake of, exogenous SA in cotyledons than in roots. Quantitative real-time reverse transcription (qRT)-PCR analysis showed that SA at 25 μM did not inhibit the expression levels of *CLC* and *CHC* mRNA in whole seedlings or roots following 30- and/or 120-min treatments (Supplemental Fig. S5, A and B).

To clarify whether lower concentrations of SA (25 μM) are sufficient to inhibit CME, we examined the effect of SA on the internalization of PM-resident proteins, including PIN2, PIP2A, and the low-temperature-induced protein RARE COLD INDUCIBLE2A (RCI2A), which was shown to be dependent on CME (Dhonukshe et al., 2007; Du et al., 2013; Wang et al., 2013a), in the presence of the vesicle-trafficking inhibitor brefeldin A (BFA; 50 μM). As shown in Supplemental Figure S6, SA at 25 μM dramatically reduced the intracellular accumulation of PIN2-, PIP2A-, and RCI2A-GFP in BFA bodies in the root cells.

TyrA23 Also Differentially Affects the Membrane Association of CHCs and CLCs

TyrA23, but not its analog tyrphostin A51 (TyrA51), interferes with CME of cargo proteins in animal and plant cells (Crump et al., 1998; Banbury et al., 2003; Ortiz-Zapater et al., 2006; Dhonukshe et al., 2007; Konopka et al., 2008; Fujimoto et al., 2010). To further explore the effect of TyrA23 on clathrin membrane recruitment, we assessed the levels of membrane-associated CLC1 and CHC in TyrA23-treated wild-type root cells by IF microscopy. Similar to the effects of SA and 2,4-D on clathrin (Fig. 2; Supplemental Fig. S3), TyrA23 (30 μM) treatment initially affected CLC1 membrane association (5–30 min; Fig. 3, A–D). However, the membrane reassociation of CLC1 in the presence of TyrA23 (restored after 120 min; Fig. 3, E and F) displayed kinetics resembling auxin (120 min; Supplemental Fig. S3) rather than SA (240 min; Fig. 2). Again, similar to the 2,4-D effects (Supplemental Fig. S3), the levels of membrane-associated CHC initially increased (after 30 min) and subsequently decreased (after 120 min; Fig. 3, G to L). TyrA51 at 30 μM (as a negative control) had no detectable effects on the levels of membrane-associated CLC1 and CHCs. TyrA23, therefore, impacts the membrane association of clathrin, consistent with its interference of CME (Dhonukshe et al., 2007).

Immunoblot analysis confirmed that TyrA23 (30 μM), in contrast to TyrA51 (30 μM), decreased the membrane-associated CLC1/2 levels but enhanced CHC levels upon 30 min of treatment (Supplemental Fig. S4C). These changes in CLC1/2 membrane association were subsequently reverted back to control levels, while CHC levels decreased 120 min after TyrA23 exposure. Consistent with these results, TyrA23 (30 and 60 μM) decreased the PM signals of CLC1/2-GFP in cotyledon epidermal cells (Supplemental Fig. S4B). qRT-PCR analysis, furthermore, showed that TyrA23 at 30 μM did not significantly affect *CLC* and *CHC* transcription upon 30- and 120-min treatments (Supplemental Fig. S5A).

SA, But Not 2,4-D, Affects the Membrane Association of the AP-2 Subunits

In addition to its effect on clathrin membrane association (Fig. 3), TyrA23 disrupts the PM association of the AP-2 complex subunits (Di Rubbo et al., 2013; Fan

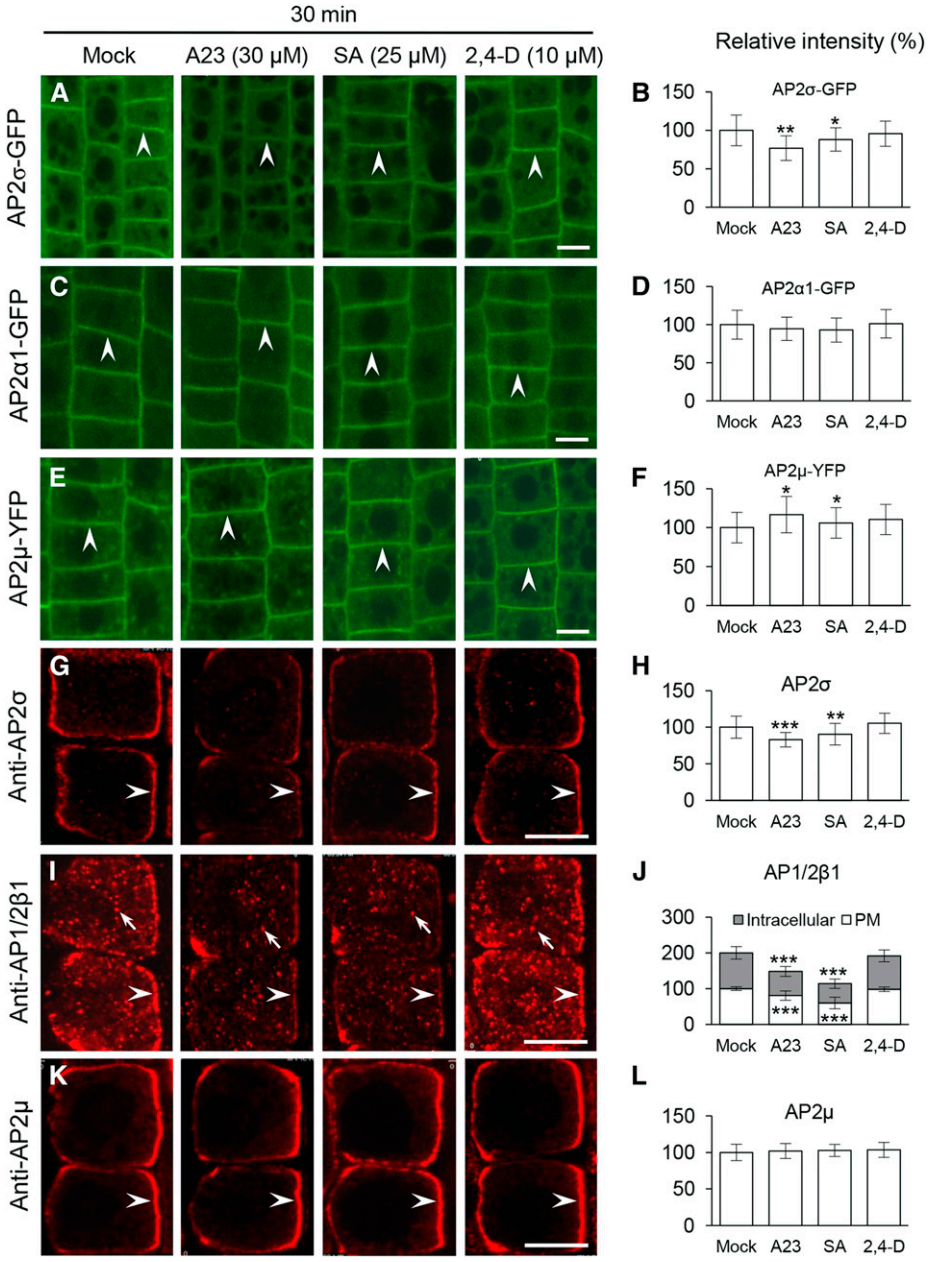

Figure 4. Impacts of CME effectors/inhibitor on the PM association of AP-2 subunits. A to F, Live-cell imaging analysis of the impacts of CME effectors/inhibitor on the PM association of fluorescently tagged AP-2 subunits. G to L, IF analysis of the impacts of CME effectors/inhibitor on AP-2 membrane association. B, D, and F show the relative intensities of fluorescently tagged AP-2 subunits at the PM (n = 160–250 cells from eight to 12 roots each). H, J, and L show the relative intensities of AP2σ, AP1/2β1, and AP2μ at the membranes (n = 61–79 cells from six to eight roots each). Treatments with DMSO (Mock), TyrA23 (A23; 30 μM), SA (25 μM), and 2,4-D (10 μM) and duration time (30 min) are indicated at the top. Arrowheads and arrows show PM-associated AP-2 subunits and intracellular compartment-associated AP1/2β1, respectively. Values shown are means ± SD. *, $P < 0.05$; **, $P < 0.001$; and ***, $P < 0.0001$ (Student's t test; compared with the mock control). Bars = 10 μm.

et al., 2013; Kim et al., 2013; Yamaoka et al., 2013). To further investigate the mechanisms by which CME effectors, auxin and SA, and a CME inhibitor, TyrA23, impact the membrane recruitment of AP-2 subunits, we examined their impacts on the PM association of the AP-2 subunits by quantitative live-cell and/or IF microscopy using affinity-purified anti-AP1/2β1, anti-AP2μ, and anti-AP2σ antibodies. Immunoblot analysis of total protein extracts from leaf tissues (Supplemental Fig. S7A) showed the absence of the 48-kD AP2μ and 15-kD AP2σ polypeptides in the *ap2*μ and *ap2*σ mutants, respectively, providing further confirmation of the specificity of anti-AP2μ and anti-AP2σ antibodies. In addition to detecting their corresponding polypeptides, anti-AP2μ and anti-AP2σ antibodies displayed cross reactions against unidentified polypeptides in the wild-type and mutant lines. However, anti-AP2μ and anti-AP2σ antibodies specifically labeled the PM in wild-type cells but not in the loss-of-function *ap2*μ and *ap2*σ mutants, respectively (Supplemental Fig. S7, B and C). In contrast to the AP2μ and AP2σ subunits, which are specific for the AP-2 complex, the AP1/2β subunits, AP1/2β1 and AP1/2β2, have been suggested to be shared by the AP-2 and AP-1 complexes (Bassham et al., 2008). Consistent with this, anti-AP1/2β1 antibodies labeled the PM (Supplemental Fig. S7D) and largely colocalized with CLC1-GFP at the intracellular compartments, as demonstrated by quantitative colocalization analysis (Supplemental Fig. S7, E–G). For the analysis of AP2α membrane recruitment, we

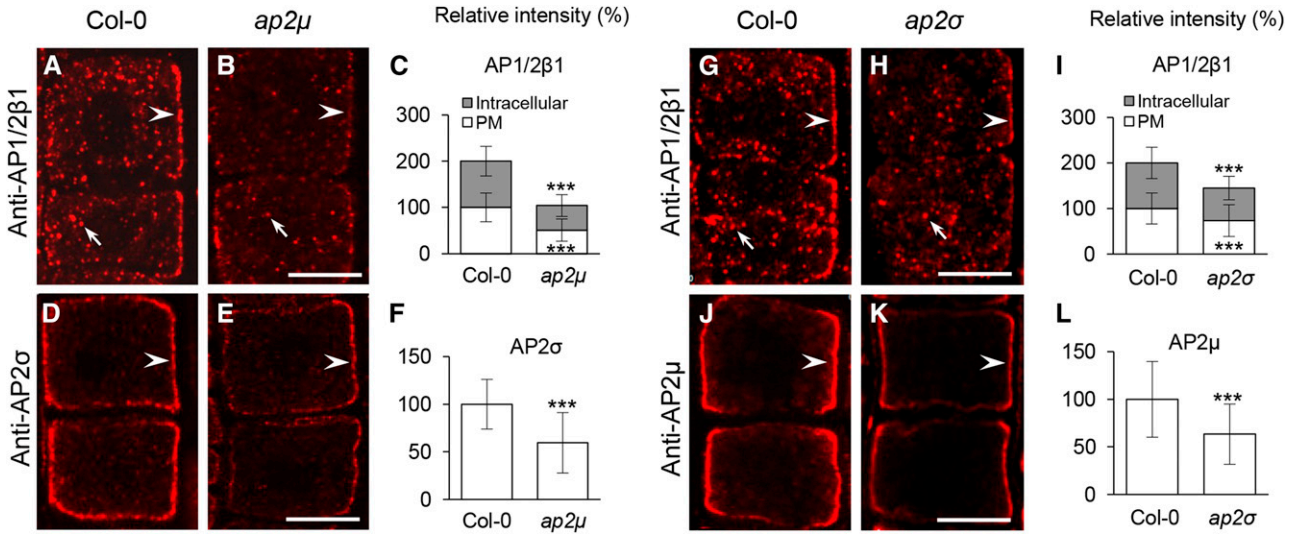

Figure 5. IF analysis of the AP-2 PM association in *ap2μ* and *ap2σ*. A to F, Effects of loss of AP2μ on the membrane association of AP1/2β1 and AP2σ. G to L, Effects of loss of AP2σ on the membrane association of AP1/2β1 and AP2μ. C, F, I, and L show the relative intensities of membrane-associated AP2 subunits (n = 72–92 cells from seven to 11 roots each; the quantitative data are summarized in Supplemental Table S2). Arrowheads and arrows show PM-associated AP-2 subunits and intracellular compartment-associated AP1/2β1, respectively. Values shown are means ± SD. ***, $P < 0.0001$ (Student's t test). Bars = 10 μm.

relied solely on the use of live-cell imaging of lines expressing AP2α1-GFP.

Previous studies have analyzed the effect of TyrA23 on AP-2 PM association using higher concentrations and/or longer treatment periods relative to the conditions we have utilized (TyrA23, 30 μM, 30 min; Fig. 3). Similar to the effects of high TyrA23 concentrations (60 and 90 μM, 30 min; Supplemental Fig. S8), SA (50 and 100 μM) affected the PM association of AP2α1-GFP, AP2μ-YFP (for yellow fluorescent protein), and AP2σ-GFP after 30 min of treatment (Supplemental Fig. S8). However, at lower concentrations of SA (25 μM) or TyrA23 (30 μM) that effectively inhibit CLC1 membrane association (Figs. 2 and 3), we observed that SA or TyrA23 had differential effects on the membrane association of fluorescent fusion protein-tagged AP-2 subunits and endogenous AP-2 subunits upon 30 min of treatment (Fig. 4). Notably, SA (25 μM) or TyrA23 (30 μM) affected the PM association of AP2σ (Fig. 4, A, B, G, and H; approximately 12% and 10% loss of AP2σ-GFP and AP2σ upon SA treatment and approximately 23% and 17% reduction upon TyrA23 treatment, respectively) as well as AP1/2β1 localization to the PM and intracellular compartments (Fig. 4, I and J; approximately 20% and 40% reduction upon TyrA23 and SA treatment, respectively; Supplemental Fig. S9A), but it did not significantly decrease PM-associated levels of AP2α1-GFP (Fig. 4, C and D) and AP2μ-YFP (Fig. 4, E and F; a slight increase) or AP2μ (Fig. 4, K and L). Furthermore, prolonged treatments (120 min) with TyrA23, but not SA, significantly decreased the levels of PM-associated AP2α1-GFP and AP2μ-YFP (Supplemental Fig. S10; AP2μ-YFP was increased slightly by SA). Additionally, the auxins 2,4-D (10 μM) and IAA (10 μM), which rapidly disrupt clathrin association with the PM and intracellular compartments (Supplemental Fig. S3; Wang et al., 2013a), did not alter the PM association of the four AP-2 subunits after 30- and/or 120-min treatments (Fig. 4; Supplemental Figs. S10 and S11). As confirmed by qRT-PCR analysis, the differential changes in the levels of PM-associated AP2σ and AP1/2β1 caused by SA or TyrA23 treatment were not due to alterations in AP-2 subunit mRNA levels (Supplemental Fig. S5C).

Membrane Association of Other AP-2 Subunits in *ap2μ* and *ap2σ*

Having shown that SA at 25 μM impacts the PM association of AP2σ and AP1/2β1, but not AP2μ and AP2α1-GFP, upon 30- and 120-min treatments (Fig. 4; Supplemental Fig. S10), we examined whether other AP-2 subunits may be recruited to the PM in *ap2μ* and *ap2σ* loss-of-function mutants, in which CME (Bashline et al., 2013; Fan et al., 2013; Kim et al., 2013) and PM-associated CLC1/2-GFP levels are reduced (Fan et al., 2013; Supplemental Fig. S12, A–F). Quantitative IF analysis showed that the levels of endogenous PM-associated AP1/2β1 and AP2σ in the *ap2μ* mutants (Fig. 5, A–F; Supplemental Table S2; Supplemental Fig. S9B) were reduced by approximately 49% and 41%, respectively, relative to the wild type, whereas in the *ap2σ* mutant lines (Fig. 5, G–L; Supplemental Table S2; Supplemental Fig. S9B), there were approximately 27% and 37% reductions of PM-associated AP1/2β1 and AP2μ levels, respectively. Similarly, loss of AP2μ caused approximately 56% and 57% reductions of PM-associated AP2α1-GFP and AP2σ-GFP levels, respectively (Supplemental Fig. S12, G–L; Supplemental Table S2), while the *ap2σ* mutants displayed approximately 37% and 32% reductions of

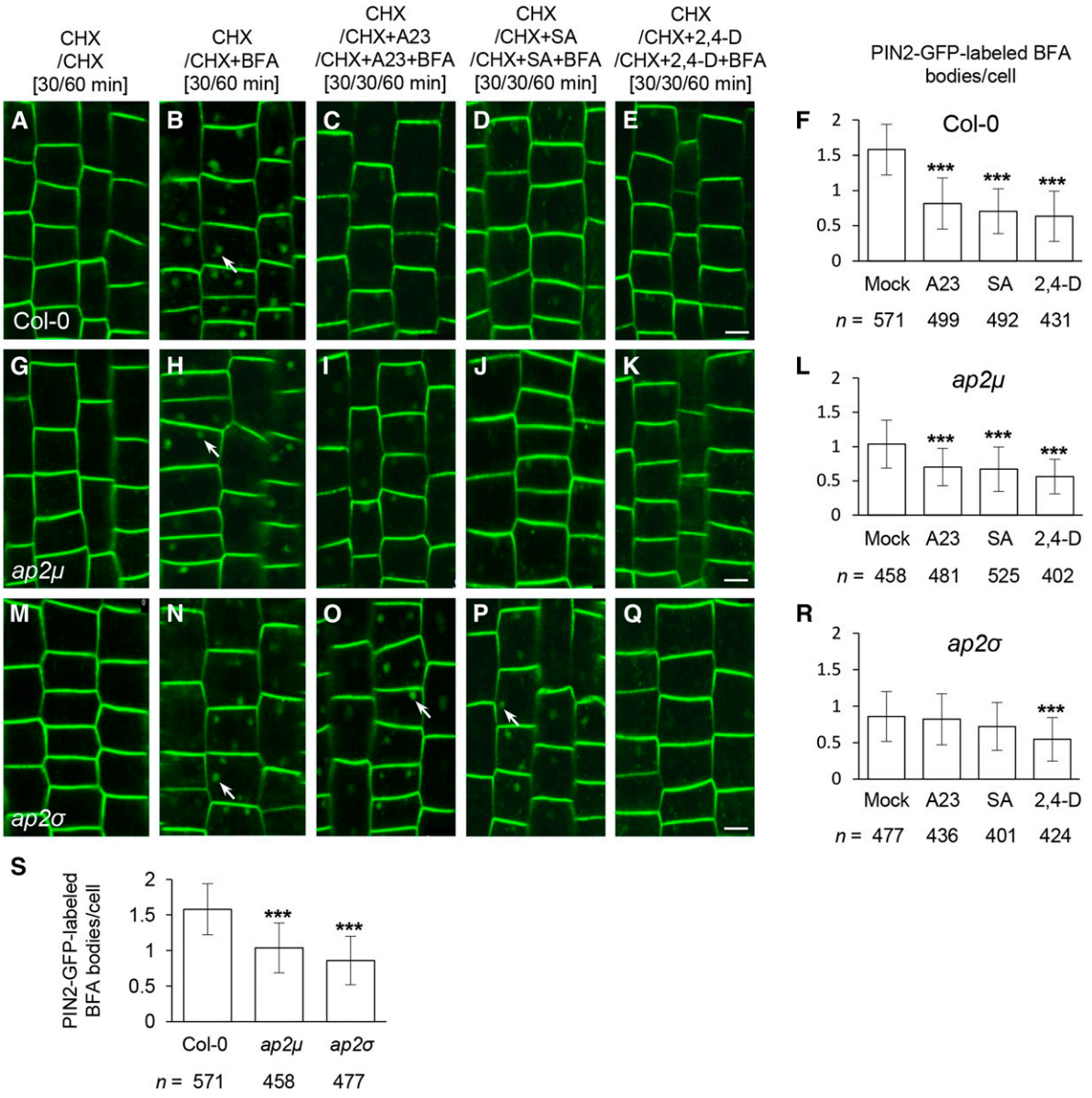

Figure 6. Interference of CME effectors/inhibitor with endocytosis in the *ap-2* mutants. A to R, Effects of TyrA23 (A23; 30 μM), SA (25 μM), and 2,4-D (10 μM) treatments on PIN2-GFP internalization in wild-type (A–F), *ap2*μ (G–L), and *ap2*σ (M–R) root cells. F, L, and R show the average number of PIN2-GFP-labeled BFA bodies in the presence of CME effectors/inhibitor. S, Average number of PIN2-GFP-labeled BFA bodies in the absence of CME effectors/inhibitor. Mock controls in F, L, and R are identical to those in D. The durations of pretreatments and treatments are indicated at the top. Arrows show PIN2-GFP-labeled BFA bodies. Values shown are means ± SD. ***, $P < 0.0001$ (Student's *t* test; compared with the mock or wild-type control). *n*, Total number of cells examined from 11 to 15 roots. Bars = 10 μm.

PM-associated AP2α1-GFP and AP2μ-YFP levels, respectively (Supplemental Fig. S12, M–R; Supplemental Table S2). These results suggest that the loss of AP2μ or AP2σ partially impacts the membrane association of other AP-2 subunits.

AP2σ Is Necessary for SA and TyrA23 Inhibition of PIN2 Internalization

As shown above, SA (25 μM) and TyrA23 (30 μM) predominantly affect the levels of PM-associated AP2σ and AP1/2β1 (Fig. 4). Thus, we expected that if other AP-2 subunits in the *ap2*μ and *ap2*σ mutants are functional during CME, loss of AP2σ, but not AP2μ, could reduce the inhibitory effects of SA and TyrA23 on CME. To test this, we examined the endocytosis of PIN2-GFP in the *ap2*μ and *ap2*σ mutants treated with or without CME effectors/inhibitor. Consistent with previous findings with reduced CME in *ap-2* mutants (Bashline et al., 2013; Fan et al., 2013; Kim et al., 2013), PIN2-GFP endocytosis was reduced in both *ap2*μ and *ap2*σ relative to wild-type cells in the presence of the protein synthesis inhibitor cycloheximide

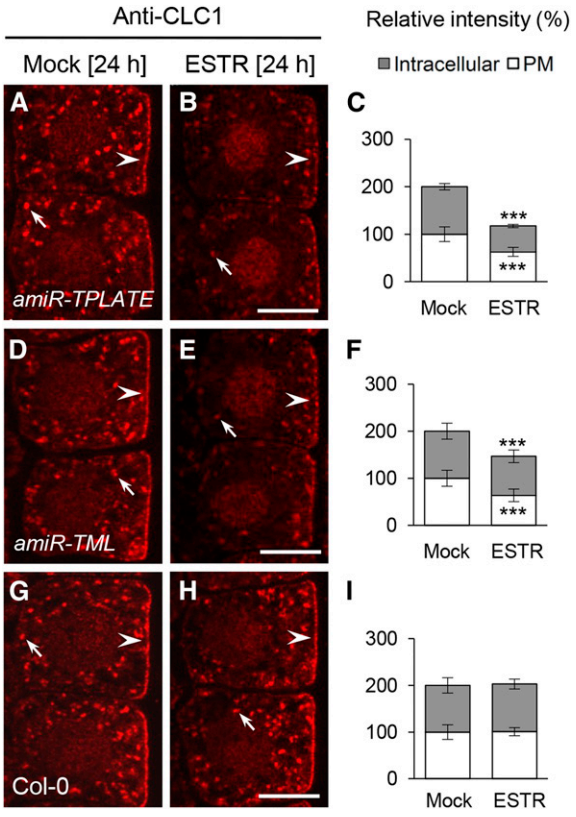

Figure 7. TPC-dependent membrane association of clathrin. IF analysis shows the PM- and intracellular compartment-associated CLC1 in ESTR-inducible *amiR-TPLATE* (A–C), *amiR-TML* (D–F), and wild-type (G–I) root cells. C, F, and I show the relative intensity of CLC1 at the PM and intracellular compartments (n = 118–199 cells from eight roots each). The duration of induction with DMSO (Mock) and ESTR (5 μM) is indicated at the top. Arrows and arrowheads show intracellular compartment- and PM-associated CLC1, respectively. Values shown are means ± SD. ***, $P < 0.0001$ (Student's t test). Bars = 7.5 μm.

(CHX) at 50 μM (Fig. 6, B, H, N, and S). Furthermore, similar to their inhibitory effects in wild-type cells (Fig. 6, B–F), TyrA23 (30 μM), SA (25 μM), and 2,4-D (10 μM) significantly inhibited PIN2-GFP endocytosis in *ap2*μ relative to mock-treated control cells (Fig. 6, H–L). By contrast, *ap2*σ mutants displayed resistance to the inhibitory effects of TyrA23 and SA, but not 2,4-D, on PIN2-GFP endocytosis (Fig. 6, N–R), compared with the wild-type and *ap2*μ cells (Fig. 6, B–F and H–L). These results provide further support for our hypothesis that SA and TyrA23 exert their inhibitory effects on CME and clathrin membrane association through individual AP-2 subunits.

Recent work showing that PIN2 endocytosis is differentially regulated between trichoblast versus atrichoblast cells in root epidermis (Löfke et al., 2015) prompted us to examine whether the loss of AP2σ or AP2μ and CME effectors/inhibitor differentially impacts PIN2 internalization in these two different cell types. As reported (Löfke et al., 2015), the average number of PIN2-GFP-labeled BFA bodies in trichoblast cells (1.73 ± 0.65) was slightly higher than that of atrichoblast cells (1.46 ± 0.46) in the wild type (Supplemental Fig. S13B). However, the loss of AP2μ or AP2σ and treatments with CME effectors/inhibitor in the wild type or *ap2*μ or *ap2*σ had a similar impact on PIN2-GFP internalization between these two types of cells relative to wild-type cells or the mock control (Supplemental Fig. S13).

The TPC Is Required for Clathrin Membrane Recruitment

AP-2 and the TPC dynamically colocalize with clathrin at the PM (Gadeyne et al., 2014), and *ap2*μ and *ap2*σ mutants show a reduction in the levels of PM-associated CLC1/2-GFP (Fan et al., 2013; Supplemental Fig. S12). To determine if the TPC is likewise required for clathrin membrane association, we examined CLC1 localization in seedlings expressing the estradiol (ESTR)-inducible artificial microRNA *amiR-TPLATE* and *amiR-TML* constructs (Gadeyne et al., 2014) by IF microscopy using affinity-purified anti-CLC1-specific antibodies. The levels of PM- and intracellular compartment-associated CLC1 were found to be reduced following ESTR (5 μM, 24 h) induction of *amiR-TPLATE* and *amiR-TML* expression relative to uninduced *amiR-TPLATE* and *amiR-TML* mock controls (Fig. 7, A–F). Estradiol treatment of wild-type Columbia-0 (Col-0) cells (Fig. 7, G–I) did not affect CLC1 membrane association. Furthermore, qRT-PCR analysis showed that ESTR treatment and/or down-regulation of *TPLATE* or *TML* (Supplemental Fig. S5D) did not decrease the transcriptional levels of *CLC1* to *CLC3* (Supplemental Fig. S5E). These results suggest that normal recruitment of clathrin to the membranes is dependent on both AP-2 complex and TPC.

The Membrane Association of the TPC Subunits Is Not Affected by Auxin and SA

The TPC is required for CME and has been proposed to function in the recruitment of clathrin triskelia and AP-2 to sites of endocytosis at the PM (Gadeyne et al., 2014; Fig. 7). To address whether the inhibition of CME by auxin, SA, and TyrA23 is mediated through the TPC, we used live-cell imaging to analyze their effects on the PM association of five fluorescently tagged subunits of the TPC, namely TPLATE, TML, TPLATE-associated SH3 domain-containing protein (TASH3), the Arabidopsis EH domain-containing protein1 (AtEH1), and AtEH2 (Van Damme et al., 2011; Gadeyne et al., 2014). In contrast to the AP-2 subunits (Fig. 4), the PM association of the TPC subunits (Fig. 8) was not detectably affected when cells were treated with 30 μM TyrA23 or 25 μM SA for 30 min, which does affect the PM association of the AP-2 subunits, AP2σ and AP1/2β1. However, consistent with the previously observed effect of TyrA23 (75 μM) on the PM association of TPLATE (Van Damme et al., 2011), increased concentrations of TyrA23 (90 μM) caused dissociation of the five fluorescently tagged TPC subunits from the PM following a 30-min treatment (Supplemental Fig. S14). In contrast, the PM association of the TPC subunits was not affected by 2,4-D (10 μM; Fig. 8) or IAA (10 μM; Supplemental Fig. S11) or by increased

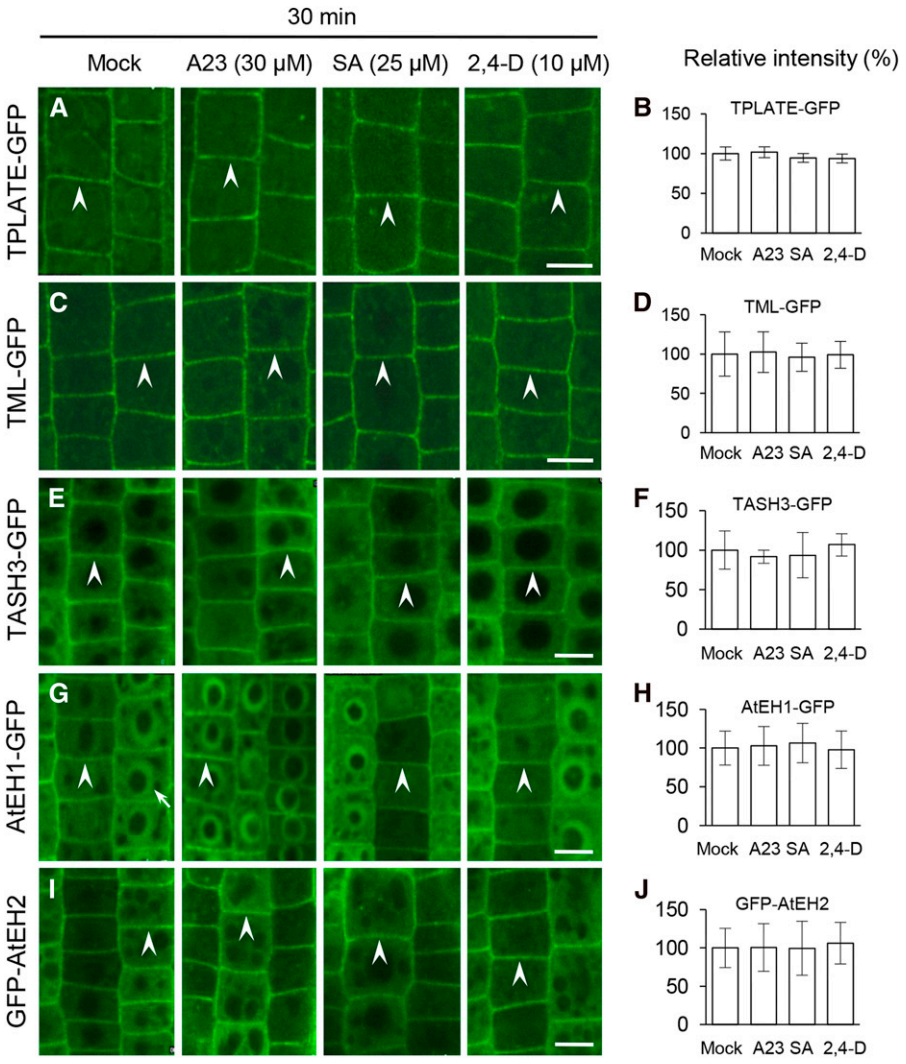

Figure 8. Impacts of CME effectors/inhibitor on the PM association of the TPC subunits. Treatments were performed with TyrA23, SA, and 2,4-D for 30 min in the seedlings expressing GFP-fused TPC subunits. B, D, F, H, and J show the relative intensities of PM-associated GFP-fused TPC subunits ($n = 61–145$ cells from four to eight roots each). Treatments with DMSO (Mock), TyrA23 (A23; 30 μM), SA (25 μM), and 2,4-D (10 μM) and duration time are indicated at the top. Arrowheads show PM-associated GFP-fused TPC subunits, whereas the arrow shows an AtEH1-GFP-labeled nucleus. Values shown are means ± SD. Bars = 10 μm.

concentrations of SA (50 and 100 μM; Supplemental Fig. S14). Taken together, these results demonstrate that auxin has no effect on either AP-2 or TPC membrane association and that SA and TyrA23 influence the PM association of AP2σ and AP1/2β1 but not AP2α1, AP2μ, and the TPC subunits.

The TPC Is Necessary for CLC Association with AP-2-Depleted Membranes

As shown above, extended TyrA23 treatment (30 μM, 120 min) resulted in the significant depletion of all four AP-2 subunits from the PM (Supplemental Fig. S10). However, under these conditions, the levels of membrane-associated CLC1/2 recovered to levels comparable to untreated cells (Fig. 3; Supplemental Fig. S4C), suggesting that CLC1/2 can bind to the PM in the absence of AP-2. Therefore, we took advantage of the ability of TyrA23 to conditionally deplete the AP-2 complex and clathrin from the membranes to investigate whether the TPC is sufficient for CLC binding to the PM in the absence of AP-2 function. For this, we used IF microscopy in TyrA23-treated TPLATE- and TML-deficient *amiR-TPLATE* and *amiR-TML* seedlings. In wild-type control cells that express endogenous levels of TPLATE and TML, ESTR treatment had no effect on TyrA23-triggered depletion and subsequent restoration of membrane-associated CLC1 (Fig. 9, A–C, J, and K). In contrast, upon a 120-min TyrA23 treatment, CLC1 restoration at the membranes was abolished in the ESTR-induced TPLATE- and TML-deficient root cells (Fig. 9, D–K). These results demonstrate that the TPC is necessary for the recruitment of clathrin to the PM following AP-2 depletion.

DISCUSSION

CME Is Dependent on Functions of AP-2 and the TPC in Plant Cells

In animal cells, the AP-2 complex is postulated to function as a central interaction hub for the recruitment of factors necessary for CCV formation and release.

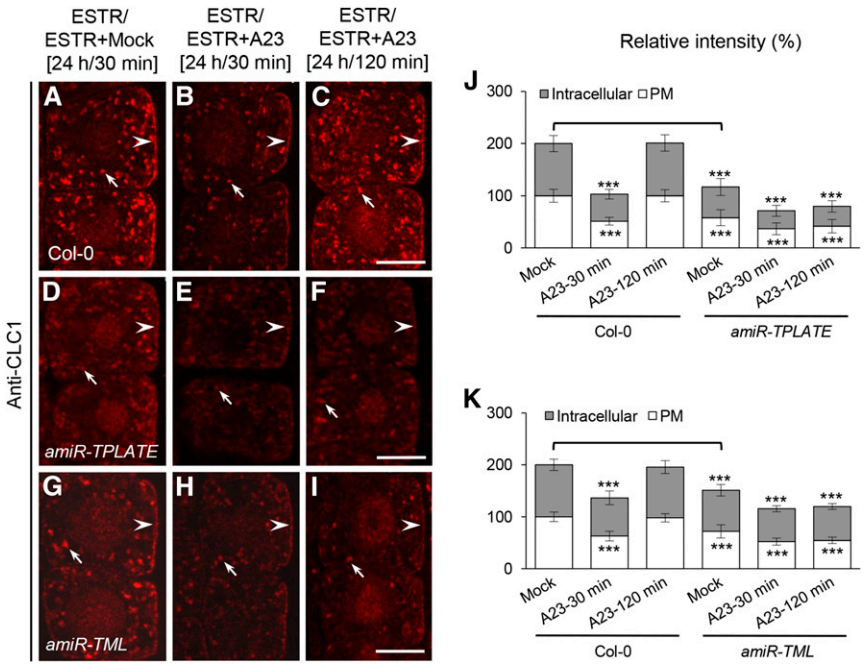

Figure 9. TPC-dependent membrane association of clathrin in AP-2-deficient cells. A to I, Effects of the down-regulation of *TPLATE* and *TML* on the membrane association of CLC1 in TyrA23-treated root cells. J and K, Relative intensities of CLC1 at the PM and intracellular compartments in *amiR-TPLATE* (J; n = 47–67 cells from eight to 11 roots each) and *amiR-TML* (K; n = 45–59 cells from six to eight roots each) lines upon TyrA23 treatment. Durations of induction with ESTR (5 μM) and treatments with DMSO (Mock) and TyrA23 (A23; 30 μM) are indicated at the top. Arrowheads and arrows show PM- and intracellular compartment-associated CLC1, respectively. Values shown are means ± SD. ***, $P < 0.0001$ (Student's t test; TyrA23 treatments versus their own mock control; the mock control in *amiR-TPLATE* and *amiR-TML* lines versus the wild-type mock control is indicated by brackets). Bars = 7.5 μm.

Nevertheless, depletion of the metazoan AP2α does not significantly impact endocytosis of the CME cargo protein, transferrin, but rather affects the dynamics of clathrin-coated pit initiation and maturation (Aguet et al., 2013), suggesting that clathrin-coated pit formation is mediated through the coordinated function of multiple and potentially partially redundant clathrin accessory factors. Indeed, CME in plant cells has been shown to be dependent on both the evolutionarily conserved AP-2 (Bashline et al., 2013; Di Rubbo et al., 2013; Fan et al., 2013; Kim et al., 2013; Yamaoka et al., 2013) and the TPC (Van Damme et al., 2011; Gadeyne et al., 2014), but how AP-2 and the TPC function together in CCV formation has not been defined.

Consistent with a role for both AP-2 and the TPC in clathrin binding to the PM, the levels of membrane-associated CLC1 and/or CLC2 were dramatically reduced in loss-of-function *ap-2* mutants (Fan et al., 2013; Supplemental Fig. S12) and in ESTR-inducible *amiR-TPLATE* and *amiR-TML* seedlings (Fig. 7). To further investigate the roles of the AP-2 complex and TPC in clathrin recruitment, we utilized the CME effector/inhibitor, SA and TyrA23, in combination with loss-of-function *ap-2* and *tpc* down-regulation mutants. The differential effects of SA or TyrA23 on the PM association of the AP-2 complex and clathrin but not the TPC (Figs. 2–4 and 8), together with the data showing that the TPC is required for CLC recruitment to AP-2-depleted membranes (Fig. 9), provide evidence that the TPC and AP-2 have independent as well as overlapping roles in the coordination of clathrin recruitment and potentially in the stabilization of the clathrin coat during CCV formation at the PM.

Additionally, although AP-2 and the TPC function in CME, we observed a loss of intracellular compartment-associated CLC1 upon exposure to CME effectors/inhibitor (Figs. 2 and 3; Supplemental Figs. S1–S3) or in *ap-2* mutants (Supplemental Fig. S12) and TPC knockdown lines (Fig. 7), suggesting that clathrin recruitment to the intracellular compartments depends on CCV activity at the PM. An alternative, but not mutually exclusive, possibility is that CLCs are degraded upon CME inhibition, thereby reducing total cellular clathrin levels.

Membrane Association and Function of the AP-2 Complex in Plant Cells

Our data indicate that the multimeric AP-2 complex and TPC jointly function in the recruitment of clathrin for CME. Previous studies, however, have demonstrated that mutations in individual TPC subunits display severe growth defects, including pollen and seedling lethality (Van Damme et al., 2006; Gadeyne et al., 2014), whereas AP-2 subunit mutants (Bashline et al., 2013; Di Rubbo et al., 2013; Fan et al., 2013; Kim et al., 2013; Yamaoka et al., 2013) exhibit only mild developmental defects. This has raised questions about the relative functional importance of the TPC versus the AP-2 complex in plant CME. It is plausible that the TPC, as it is an evolutionarily ancient adaptor complex (Zhang et al., 2015), is sufficient to support basic CME levels required for plant cell function. Alternatively, *ap-2* mutants lacking only a single subunit may still form partial AP2 complexes that retain some level of activity necessary for CME. Consistent with this hypothesis, we found that remaining AP-2 subunits can associate with the PM in Arabidopsis single *ap-2* subunit mutants (Fig. 5; Supplemental Fig. S12; Supplemental Table S1). Furthermore, SA or TyrA23 caused differences in the PM association of individual

AP-2 subunits (Fig. 4) and in the endocytosis of PM-associated PIN2 in *ap2σ* and *ap2μ* mutant lines (Fig. 6), suggesting that plant AP-2 subunits can assemble independently or in partially functional subcomplexes. In a related manner, it was recently shown that *C. elegans* mutants, which are defective in a single AP-2 subunit, exhibit only a modest reduction in CME, likely due to the formation of partially active AP-2 complexes (Gu et al., 2013).

Differential Regulation of CME by Auxin, SA, and TyrA23

Clathrin triskelia are composed of CLCs and CHCs. Nonetheless, the initial loss of membrane-associated CLC in plant cells treated with auxin, SA, and TyrA23 was accompanied by a transient but pronounced increase in the levels of membrane-associated CHC, which was followed by its membrane dissociation (Figs. 2 and 3; Supplemental Figs. S3 and S4). Loss of CLC, and potentially other clathrin-associated factors, may thus affect the CHC membrane dynamics necessary for the productive formation of endocytic CCVs. Short-term treatments (5 or 30 min) with low concentrations of SA (25 μM) and TyrA23 (30 μM), which are sufficient to block CME (Dhonukshe et al., 2007; Fig. 6; Supplemental Fig. S6), enabled us to dissect how these CME effectors/inhibitor impact the PM association of clathrin and its adaptor proteins. Our data suggest that SA and TyrA23, but not auxin, inhibit the clathrin PM association via AP-2, in particular through the PM association of the AP2σ and AP1/2β1 subunits (Fig. 4), and not via the TPC (Fig. 8). Furthermore, as the PM localization of the TPC (Fig. 8) is not affected by auxin, SA, or TyrA23, the PM dissociation of clathrin in response to these CME effectors/inhibitor is not mediated through the TPC. Together, these data suggest that, in plants, endogenous developmental and defense signals such as auxin and SA may differentially modulate the membrane recruitment of clathrin and components of the clathrin-related machinery and, thereby, regulate the process of CME in plant cells.

SA and TyrA23 show highly similar effects on the membrane association of clathrin and AP-2 subunits (Figs. 2–4; Supplemental Fig. S8). However, a notable difference is that TyrA23 (75 μM or greater; Van Damme et al., 2011; Supplemental Fig. S14), but not SA (100 μM; Supplemental Fig. S14), resulted in TPC dissociation from the PM, suggesting that TyrA23 has additional effects on the process of CME at high concentrations compared with SA. Indeed, TyrA23 (100 μM) inhibits flg22-elicited reactive oxygen species formation (Smith et al., 2014a, 2014b), indicating that TyrA23 affects not only CME but other biochemical and/or cellular processes in a dose-dependent manner. Thus, it is important to evaluate the effects of TyrA23 over a range of concentrations and incubation times to discriminate its effect on different, and potentially overlapping, cellular processes.

A major question that remains to be addressed is the molecular mechanisms by which auxin and SA regulate the PM association of clathrin and/or AP-2. Given that auxin does not affect the membrane association of the AP-2 complex or the TPC, auxin signaling may directly negatively regulate the recruitment and/or dynamics of clathrin and, consequently, CME through cell surface-localized AUXIN-BINDING PROTEIN1 (ABP1)-mediated signaling (Robert et al., 2010; Xu et al., 2010) via the auxin-sensing receptor-like kinase complex (Xu et al., 2014). This model, however, does not preclude a role for other factors that may be required for the auxin regulation of clathrin function during CME. Indeed, the recent finding that *abp1* mutants show no gross growth defects (Enders et al., 2015; Gao et al., 2015) warrants further study of the role of ABP1 in the auxin-dependent regulation of CME. Recent studies showing that SA inhibition of plant CME is independent of SA receptor-mediated transcription (NONEXPRESSER OF PR GENES3/4; Du et al., 2013) support the SA inhibition of CME via an untranscriptional mechanism. Based on the rapid effects of auxin and SA on plant CME, it is more likely that they regulate the membrane association of clathrin and/or AP-2 subunits and, thereby, CME via rapid posttranslational modifications (e.g. phosphorylation and/or dephosphorylation). Additionally, the various CLC (CLC1, CLC2, and CLC3) and CHC (CHC1 and CHC2) isoforms may undergo differential regulation.

Therefore, for future study, analyses of the functions of the individual CLC and CHC isoforms and the potential role of posttranslational modifications in the regulation of the CME machinery upon auxin or SA treatment will likely be necessary to understand how developmental signals regulate CME in plants.

MATERIALS AND METHODS

Plant Material and Growth Conditions

The following Arabidopsis (*Arabidopsis thaliana*) transgenic lines and mutants were used in this study: *ProWOX5:IAAH* (Blilou et al., 2005), *Pro-35S:CLC1-GFP* (Wang et al., 2013a), *ProCLC2:CLC2-GFP* (Konopka et al., 2008; Ito et al., 2012), *ProAP2μ:AP2μ-YFP* (Bashline et al., 2013), *Pro-35S:AP2α1-GFP* (*AP2A1-GFP*; Di Rubbo et al., 2013), *ProAP2σ:AP2σ-GFP/ap2σ* (Fan et al., 2013), *ProPIN2:PIN2-GFP* (Xu and Scheres, 2005), *ProLAT52:TPLATE-GFP* (Van Damme et al., 2006), *ProTML:TML-GFP*, *Pro-35S:TASH3-GFP*, *Pro-35S:AtEH1-GFP*, *Pro-35S:GFP-AtEH2*, and ESTR-inducible *ProESTR:amiR-TPLATE* (Col-0 background) and *ProESTR:amiR-TML/BRI1-GFP* (*ProBRI1:BRI1-GFP* background; Gadeyne et al., 2014) transgenic lines as well as *ap2σ* (SALK_141555; Fan et al., 2013) and *ap2μ* (SALK_083693C from the Arabidopsis Biological Resource Center) mutants. The homozygous *ap2μ* mutant was identified by PCR (Supplemental Table S3) and described previously (Bashline et al., 2013; Kim et al., 2013). Fluorescently tagged marker lines were crossed into *ap2σ* and *ap2μ* mutants, and the resulting homozygous lines were confirmed by PCR- and fluorescent signal-based assays.

Seeds were surface sterilized and imbibed for 3 d at 4°C in the dark and then sown onto 0.5× Murashige and Skoog (MS) 1.5% (w/v) agar plates. Seedlings were vertically grown on plates in a climate-controlled growth room (22°C/20° C day/night temperature, 16/8-h photoperiod, and 80 $\mu E\ s^{-1}\ m^{-2}$ light intensity). Five-day-old seedlings with healthy roots were used in this study, unless specified otherwise.

Chemical Solutions and Treatments

All reagents, unless specified, were from Sigma-Aldrich. DMSO was used to dissolve IAM (5 mM), SA (100 mM), IAA (10 mM), 2,4-D (10 mM), TyrA23 (30 mM), TyrA51 (30 mM), CHX (50 mM), BFA (50 mM; Invitrogen), and ESTR (20 mM) for stock solutions. Unless indicated otherwise in the text, final working

concentrations were 5 μM for IAM and ESTR, 10 μM for IAA and 2,4-D, 25 μM for SA, 30 μM for TyrA23 and TyrA51, and 50 μM for CHX and BFA.

All pretreatment and posttreatment time durations are indicated in the text. All pretreatments and treatments for subcellular localization of membrane-associated proteins were performed in liquid medium (0.5× MS basal salts, 1% Suc, and 0.05% MES [w/v], pH 5.6–5.8), except the specified cases. For the induction of *amiR-TPLATE* and *amiR-TML*, 4-d-old vertically grown seedlings from 0.5× MS 1.5% (w/v) agar plates were incubated for 24 h in 0.5× MS liquid medium containing 5 μM ESTR as described previously (Gadeyne et al., 2014) or followed by treatment with ESTR plus TyrA23 (30 μM). The resulting materials were used in IF analysis and/or qRT-PCR assay.

Polyclonal Antibodies and Immunoblot Analysis of the AP-2 Subunits

Polyclonal antibodies of the AP-2 subunits, including anti-AP1/2β1, anti-AP2μ, and anti-AP2σ, were raised in rabbits using synthesized peptides related to each protein (Supplemental Table S4) coupled with keyhole limpet hemocyanin containing an additional N-terminal Cys (HUABIO). Antibodies were affinity purified using immobilized-peptide affinity columns. To verify the specificity of anti-AP2μ (1:500 dilution) and anti-AP2σ (1:500 dilution), total protein extracts (20 μg loading for each sample) from leaf tissues of Col-0, *ap2*μ, and *ap2*σ adult plants were used for immunoblot analysis (Supplemental Fig. S7A). However, loss-of-function *ap1/2*β*1* mutants are not currently available with which to test the specificity of the anti-AP1/2β1 peptide antibody by immunoblot analysis.

Membrane Protein Isolation and Immunoblot Analysis of Clathrin

For the membrane-associated clathrin assay, microsomal membrane fractions were prepared as described previously (Abas et al., 2006). Briefly, approximately 1 g of 5-d-old whole seedlings grown in 0.5× MS liquid medium under continuous light was homogenized in extraction buffer (50 mM Tris [pH 6.8], 5% [v/v] glycerol, 1.5% [w/v] polyvinylpolypyrrolidone, 5 mM EGTA [pH 8], 5 mM EDTA [pH 8], 150 mM KCl, 1 mM dithioerythritol, 50 mM NaF, 20 mM β-glycerol phosphate, 0.5% [w/v] casein, protease inhibitors including 1 mM benzamidine, 1 μg mL^{-1} aprotinin, 1 μg mL^{-1} leupeptin, 5 μg mL^{-1} E64, 1 μg mL^{-1} pepstatin A, 1 mM phenylmethylsulfonyl fluoride, and one Roche Complete Mini Protease Inhibitor tablet) on ice and spun at 3,800*g* for 15 min at 4°C. The supernatant was filtered and spun (3,800*g*) again and then centrifuged (100,000*g*) for 90 min at 4°C. The pellet was resuspended in resuspension buffer (50 mM Tris [pH 7.5], 20% [v/v] glycerol, 2 mM EGTA, 2 mM EDTA, 0.5 mM dithioerythritol, 10 μg mL^{-1} casein, and protease inhibitors as above). The final samples were detected using the Bio-Rad protein assay to calculate the concentration (μg μL^{-1}).

For immunoblot analysis, the generation and purification of polyclonal antibodies, including anti-AtCLC1, anti-AtCLC2, and anti-AtCHC (1:1,000 dilution), and their detailed information have been described previously (McMichael et al., 2013; Wang et al., 2013a). Coomassie Brilliant Blue R250 staining was used as a loading control for total microsomal membrane proteins (15 μg loading for each sample). For the band intensity assay, each blot was quantified by one-dimensional gel of ImageJ software (http://rsb.info.nih.gov/ij/). The resulting data were calculated relative to the loading controls and subsequently normalized to the corresponding mock control (each mock control was set as 1).

Confocal Microscopy, Immunodetection, and Quantification

Immunolocalization studies were performed in the primary roots as described before (Sauer et al., 2006; Wang et al., 2013a). Primary antibodies against CLC1 (1:150 dilution), CHC (1:150 dilution), AP1/2β1 (1:100 dilution), AP2μ (1:100 dilution), and AP2σ (1:100 dilution) were detected using Cy3-labeled anti-rabbit secondary antibodies (Sigma-Aldrich; 1:100 dilution). Images were captured using confocal laser scanning microscope (Leica TCS SP5 AOBS). For imaging Cy3, the 543-nm line of the helium/neon laser was used for excitation, and emission was detected at 550 to 570 nm. For live-cell imaging of GFP and YFP, the 488- and 514-nm lines of the argon laser were used for excitation, and emission was detected at 496 to 532 and 520 to 560 nm, respectively. For quantitative measurement of fluorescence intensities, laser, pinhole, and gain settings of the confocal microscope were identical among different treatments or genotypes.

To quantify the intensities of fluorescence signals at the PM or intracellular compartments, digital images were analyzed using ImageJ software. Briefly, PM-associated levels of GFP- or YFP-fused or Cy3-labeled secondary antibody-detected proteins, including CLC1/2, CHC, and the AP-2 and TPC subunits, were determined by regions of interest (ROIs) using the rectangle and/or freehand line tools of ImageJ software. The levels of intracellular compartment-associated CLC1/2 and CHCs were determined by measuring multiple ROIs as their total intracellular fluorescence intensities to exclude the nuclear signals or other nonspecific background signals. The resulting data were normalized to the corresponding wild-type or mock control (100%), and the relative fluorescence intensities (%) are presented. For the quantification of AP1/2β1 intracellular signals, the total intracellular intensity using multiple ROIs and the amounts of anti-AP1/2β1 antibody-labeled intracellular compartments by counting were used. For intracellular colocalization of AP1/2β1 with CLC1-GFP, five independent confocal images were analyzed using Pearson and Spearman correlation coefficients in the colocalization plug-in of ImageJ as described previously (French et al., 2008; https://www.cpib.ac.uk/tools-resources/software/psc-colocalization-plugin/; a default threshold of 40). To reduce any background effect, ROIs were used for the colocalization assay. For measurements of the BFA-induced internalization of PIN2-GFP, the levels of internalized PIN2-GFP were presented as the average number of GFP-labeled BFA bodies per cell (Robert et al., 2010; Wang et al., 2013a). To further explore the effects of the loss of AP2μ and AP2σ on PIN2-GFP internalization in trichoblast and atrichoblast cells, amounts of GFP-labeled BFA were counted separately in these two types of cells. All confocal experiments were independently repeated at least three times, and quantitative data were statistically evaluated using Student's *t* test (paired with two-tailed distribution). Amounts of the examined seedlings and cells are indicated in the text.

Quantitative IF Analysis of Clathrin Membrane Association in Gravistimulated Roots

For gravitropic stimulation, vertically grown seedlings were gravistimulated for 2 h with 90° rotation as described previously (Pan et al., 2009). To fairly evaluate the levels of membrane-associated CLC1 at both sides of the root, higher magnification images were slightly focused before being captured from the overview images of the root during confocal imaging. These higher magnification images were used in quantitative analysis as described above.

qRT-PCR Assay

To evaluate the impact of CME effectors on the gene expression of clathrin and the AP-2 subunits, 5-d-old vertically grown whole seedlings (Col-0) were used upon treatment with DMSO (mock), TyrA23 (30 μM), SA (25 μM), and/or 2,4-D (10 μM) in 0.5× MS liquid medium for 30 and 120 min. For analysis of the effect of SA on clathrin gene expression in the roots, 10-mm root tips were incised from the seedlings treated with 25 μM SA for 30 min. For gene expression of *CLC1-3*, *TPLATE*, and *TML*, ESTR treatment conditions were described above. The resulting materials were used to isolate total RNA with the RNeasy Plant Mini Kit (Qiagen).

For qRT-PCR assay, the first-strand synthesis of complementary DNA was performed with the SuperScript III First-Strand Synthesis System (Invitrogen). The qRT-PCR assay was performed with Thunderbird SYBR qPCR mix (Toyobo) and the StepOnePlus Real-Time PCR System (Applied Biosystems). Reactions were performed in a 20-μL volume that contained 10 μL of 2× SYBR qPCR mix (Toyobo), 10 ng of complementary DNA, and 1 μM of each gene-specific primer (Supplemental Table S3; Wang et al., 2013a). PCR cycles were performed as follows: 95°C for 5 min, and then 40 cycles of 95°C for 5 s and 60°C for 50 s. The resulting data were collected and analyzed using StepOne Software version 2.1. The housekeeping genes *UBIQUITIN7* and *ACTIN2* served as normalization references for clathrin/AP-2 subunits and *TPLATE*/*TML*, respectively (Supplemental Table S3). For statistical analysis (Student's *t* test, paired with two-tailed distribution), the transcription levels were compared with the corresponding mock or wild-type control.

Sequence data from this article can be found in the Arabidopsis Genome Initiative under the following accession numbers: *CLC1* (At2g20760), *CLC2* (At2g40060), *CLC3* (At3g51890), *CHC1* (At3g11130), *CHC2* (At3g08530), *AP2*α*1* (At5g22770), *AP1/2*β*1* (At4G11380), *AP2*μ (At5g46630), *AP2*σ (At1g47830), *TPLATE* (At3g01780), *TML* (At5g57460), *TASH3* (At2g07360), *AtEH1* (At1g20760), *AtEH2* (At1g21630), *PIN2* (AT5g57090), *UBIQUITIN7* (AT2g35635), and *ACTIN2* (At3g18780).

Supplemental Data

The following supplemental materials are available.

Supplemental Figure S1. Elevation of endogenous auxin levels affects clathrin membrane association.

Supplemental Figure S2. Time-course analyses of the SA effect on CLC1-GFP membrane association.

Supplemental Figure S3. Kinetic effects of auxin on the membrane association of clathrin.

Supplemental Figure S4. Immunoblot and live-cell imaging analyses of clathrin membrane association.

Supplemental Figure S5. qRT-PCR analysis of transcriptional levels of clathrin and the AP-2/TPC subunits.

Supplemental Figure S6. Effects of low concentrations of SA on the internalization of PM proteins.

Supplemental Figure S7. Immunoblot and IF analyses of the AP-2 antibodies.

Supplemental Figure S8. Effects of high concentrations of TyrA23 and SA on the PM association of AP-2 subunits.

Supplemental Figure S9. Quantification analysis of AP1/2β1 intracellular signals in Figures 4 and 5.

Supplemental Figure S10. Impacts of CME effectors/inhibitor on the PM association of AP-2 subunits in extended treatment.

Supplemental Figure S11. Exogenous IAA effect on the PM association of the AP-2 and TPC subunits.

Supplemental Figure S12. Membrane association of clathrin and AP-2 subunits in *ap2*σ and *ap2*μ.

Supplemental Figure S13. Quantification analysis of PIN2 endocytosis in trichoblast and atrichoblast cells in Figure 6.

Supplemental Figure S14. Effects of high concentrations of TyrA23 and SA on the PM association of the TPC subunits.

Supplemental Table S1. Frequency distribution for the ratios of membrane-associated CLC1 at both sides of roots.

Supplemental Table S2. Summary of the effects of loss of AP2μ or AP2σ on the PM association of other AP-2 subunits.

Supplemental Table S3. PCR primer sequences for qRT-PCR and genotyping.

Supplemental Table S4. Information for the AP-2 antibodies.

ACKNOWLEDGMENTS

We thank Eugenia Russinova, Ikuko Hara-Nishimura, Inhwan Hwang, Takashi Ueda, Ben Scheres, Klaus Palme, Jiri Friml, Jian Xu, and Yinong Yang for generously sharing published materials and/or comments, the Arabidopsis Biological Resource Center at Ohio State University for seed stocks, and other laboratory members for their constructive discussion and help.

Received November 19, 2015; accepted March 3, 2016; published March 4, 2016.

LITERATURE CITED

Abas L, Benjamins R, Malenica N, Paciorek T, Wiśniewska J, Moulinier-Anzola JC, Sieberer T, Friml J, Luschnig C (2006) Intracellular trafficking and proteolysis of the Arabidopsis auxin-efflux facilitator PIN2 are involved in root gravitropism. Nat Cell Biol **8:** 249–256

Aguet F, Antonescu CN, Mettlen M, Schmid SL, Danuser G (2013) Advances in analysis of low signal-to-noise images link dynamin and AP2 to the functions of an endocytic checkpoint. Dev Cell **26:** 279–291

Baisa GA, Mayers JR, Bednarek SY (2013) Budding and braking news about clathrin-mediated endocytosis. Curr Opin Plant Biol **16:** 718–725

Banbury DN, Oakley JD, Sessions RB, Banting G (2003) Tyrphostin A23 inhibits internalization of the transferrin receptor by perturbing the interaction between tyrosine motifs and the medium chain subunit of the AP-2 adaptor complex. J Biol Chem **278:** 12022–12028

Barberon M, Zelazny E, Robert S, Conéjéro G, Curie C, Friml J, Vert G (2011) Monoubiquitin-dependent endocytosis of the iron-regulated transporter 1 (IRT1) transporter controls iron uptake in plants. Proc Natl Acad Sci USA **108:** E450–E458

Bashline L, Li S, Anderson CT, Lei L, Gu Y (2013) The endocytosis of cellulose synthase in Arabidopsis is dependent on μ2, a clathrin-mediated endocytosis adaptin. Plant Physiol **163:** 150–160

Bassham DC, Brandizzi F, Otegui MS, Sanderfoot AA (2008) The secretory system of Arabidopsis. The Arabidopsis Book **6:** e0116 doi: 10.1199/tab.0116

Beck M, Zhou J, Faulkner C, MacLean D, Robatzek S (2012) Spatio-temporal cellular dynamics of the *Arabidopsis* flagellin receptor reveal activation status-dependent endosomal sorting. Plant Cell **24:** 4205–4219

Bitsikas V, Corrêa IR Jr, Nichols BJ (2014) Clathrin-independent pathways do not contribute significantly to endocytic flux. eLife **3:** e03970

Blilou I, Xu J, Wildwater M, Willemsen V, Paponov I, Friml J, Heidstra R, Aida M, Palme K, Scheres B (2005) The PIN auxin efflux facilitator network controls growth and patterning in Arabidopsis roots. Nature **433:** 39–44

Chen X, Irani NG, Friml J (2011) Clathrin-mediated endocytosis: the gateway into plant cells. Curr Opin Plant Biol **14:** 674–682

Crump CM, Williams JL, Stephens DJ, Banting G (1998) Inhibition of the interaction between tyrosine-based motifs and the medium chain subunit of the AP-2 adaptor complex by specific tyrphostins. J Biol Chem **273:** 28073–28077

Dettmer J, Friml J (2011) Cell polarity in plants: when two do the same, it is not the same.... Curr Opin Cell Biol **23:** 686–696

Dhonukshe P, Aniento F, Hwang I, Robinson DG, Mravec J, Stierhof YD, Friml J (2007) Clathrin-mediated constitutive endocytosis of PIN auxin efflux carriers in *Arabidopsis*. Curr Biol **17:** 520–527

Di Rubbo S, Irani NG, Kim SY, Xu ZY, Gadeyne A, Dejonghe W, Vanhoutte I, Persiau G, Eeckhout D, Simon S, et al (2013) The clathrin adaptor complex AP-2 mediates endocytosis of *brassinosteroid insensitive1* in *Arabidopsis*. Plant Cell **25:** 2986–2997

Du Y, Tejos R, Beck M, Himschoot E, Li H, Robatzek S, Vanneste S, Friml J (2013) Salicylic acid interferes with clathrin-mediated endocytic protein trafficking. Proc Natl Acad Sci USA **110:** 7946–7951

Enders TA, Oh S, Yang Z, Montgomery BL, Strader LC (2015) Genome sequencing of *Arabidopsis abp1-5* reveals second-site mutations that may affect phenotypes. Plant Cell **27:** 1820–1826

Fan L, Hao H, Xue Y, Zhang L, Song K, Ding Z, Botella MA, Wang H, Lin J (2013) Dynamic analysis of *Arabidopsis* AP2 σ subunit reveals a key role in clathrin-mediated endocytosis and plant development. Development **140:** 3826–3837

Fan L, Li R, Pan J, Ding Z, Lin J (2015) Endocytosis and its regulation in plants. Trends Plant Sci **20:** 388–397

French AP, Mills S, Swarup R, Bennett MJ, Pridmore TP (2008) Colocalization of fluorescent markers in confocal microscope images of plant cells. Nat Protoc **3:** 619–628

Fujimoto M, Arimura S, Ueda T, Takanashi H, Hayashi Y, Nakano A, Tsutsumi N (2010) *Arabidopsis* dynamin-related proteins DRP2B and DRP1A participate together in clathrin-coated vesicle formation during endocytosis. Proc Natl Acad Sci USA **107:** 6094–6099

Gadeyne A, Sánchez-Rodríguez C, Vanneste S, Di Rubbo S, Zauber H, Vanneste K, Van Leene J, De Winne N, Eeckhout D, Persiau G, et al (2014) The TPLATE adaptor complex drives clathrin-mediated endocytosis in plants. Cell **156:** 691–704

Gao Y, Zhang Y, Zhang D, Dai X, Estelle M, Zhao Y (2015) Auxin binding protein 1 (ABP1) is not required for either auxin signaling or Arabidopsis development. Proc Natl Acad Sci USA **112:** 2275–2280

Gu M, Liu Q, Watanabe S, Sun L, Hollopeter G, Grant BD, Jorgensen EM (2013) AP2 hemicomplexes contribute independently to synaptic vesicle endocytosis. eLife **2:** e00190

Hao H, Fan L, Chen T, Li R, Li X, He Q, Botella MA, Lin J (2014) Clathrin and membrane microdomains cooperatively regulate RbohD dynamics and activity in *Arabidopsis*. Plant Cell **26:** 1729–1745

Hirst J, Schlacht A, Norcott JP, Traynor D, Bloomfield G, Antrobus R, Kay RR, Dacks JB, Robinson MS (2014) Characterization of TSET, an ancient and widespread membrane trafficking complex. eLife **3:** e02866

Holstein SEH (2002) Clathrin and plant endocytosis. Traffic **3:** 614–620

Hwang I, Robinson DG (2009) Transport vesicle formation in plant cells. Curr Opin Plant Biol **12:** 660–669

Irani NG, Di Rubbo S, Mylle E, Van den Begin J, Schneider-Pizoń J, Hniliková J, Šíša M, Buyst D, Vilarrasa-Blasi J, Szatmári AM, et al (2012) Fluorescent castasterone reveals BRI1 signaling from the plasma membrane. Nat Chem Biol **8:** 583–589

Ito E, Fujimoto M, Ebine K, Uemura T, Ueda T, Nakano A (2012) Dynamic behavior of clathrin in *Arabidopsis thaliana* unveiled by live imaging. Plant J **69:** 204–216

Kim SY, Xu ZY, Song K, Kim DH, Kang H, Reichardt I, Sohn EJ, Friml J, Juergens G, Hwang I (2013) Adaptor protein complex 2-mediated endocytosis is crucial for male reproductive organ development in *Arabidopsis*. Plant Cell **25:** 2970–2985

Kirchhausen T (2012) Bending membranes. Nat Cell Biol **14:** 906–908

Kirchhausen T, Owen D, Harrison SC (2014) Molecular structure, function, and dynamics of clathrin-mediated membrane traffic. Cold Spring Harb Perspect Biol **6:** a016725

Kitakura S, Vanneste S, Robert S, Löfke C, Teichmann T, Tanaka H, Friml J (2011) Clathrin mediates endocytosis and polar distribution of PIN auxin transporters in *Arabidopsis*. Plant Cell **23:** 1920–1931

Konopka CA, Backues SK, Bednarek SY (2008) Dynamics of *Arabidopsis* dynamin-related protein 1C and a clathrin light chain at the plasma membrane. Plant Cell **20:** 1363–1380

Lam SK, Siu CL, Hillmer S, Jang S, An G, Robinson DG, Jiang L (2007a) Rice SCAMP1 defines clathrin-coated, trans-Golgi-located tubular-vesicular structures as an early endosome in tobacco BY-2 cells. Plant Cell **19:** 296–319

Lam SK, Tse YC, Robinson DG, Jiang L (2007b) Tracking down the elusive early endosome. Trends Plant Sci **12:** 497–505

Löfke C, Scheuring D, Dünser K, Schöller M, Luschnig C, Kleine-Vehn J (2015) Tricho- and atrichoblast cell files show distinct PIN2 auxin efflux carrier exploitations and are jointly required for defined auxin-dependent root organ growth. J Exp Bot **66:** 5103–5112

McMahon HT, Boucrot E (2011) Molecular mechanism and physiological functions of clathrin-mediated endocytosis. Nat Rev Mol Cell Biol **12:** 517–533

McMichael CM, Reynolds GD, Koch LM, Wang C, Jiang N, Nadeau J, Sack FD, Gelderman MB, Pan J, Bednarek SY (2013) Mediation of clathrin-dependent trafficking during cytokinesis and cell expansion by *Arabidopsis* stomatal cytokinesis defective proteins. Plant Cell **25:** 3910–3925

Ortiz-Zapater E, Soriano-Ortega E, Marcote MJ, Ortiz-Masiá D, Aniento F (2006) Trafficking of the human transferrin receptor in plant cells: effects of tyrphostin A23 and brefeldin A. Plant J **48:** 757–770

Paciorek T, Zazímalová E, Ruthardt N, Petrásek J, Stierhof YD, Kleine-Vehn J, Morris DA, Emans N, Jürgens G, Geldner N, et al (2005) Auxin inhibits endocytosis and promotes its own efflux from cells. Nature **435:** 1251–1256

Pan J, Fujioka S, Peng J, Chen J, Li G, Chen R (2009) The E3 ubiquitin ligase $SCF^{TIR1/AFB}$ and membrane sterols play key roles in auxin regulation of endocytosis, recycling, and plasma membrane accumulation of the auxin efflux transporter PIN2 in *Arabidopsis thaliana*. Plant Cell **21:** 568–580

Park M, Song K, Reichardt I, Kim H, Mayer U, Stierhof YD, Hwang I, Jürgens G (2013) *Arabidopsis* μ-adaptin subunit AP1M of adaptor protein complex 1 mediates late secretory and vacuolar traffic and is required for growth. Proc Natl Acad Sci USA **110:** 10318–10323

Rivas-San Vicente M, Plasencia J (2011) Salicylic acid beyond defence: its role in plant growth and development. J Exp Bot **62:** 3321–3338

Robert S, Kleine-Vehn J, Barbez E, Sauer M, Paciorek T, Baster P, Vanneste S, Zhang J, Simon S, Čovanová M, et al (2010) ABP1 mediates auxin inhibition of clathrin-dependent endocytosis in *Arabidopsis*. Cell **143:** 111–121

Sauer M, Paciorek T, Benková E, Friml J (2006) Immunocytochemical techniques for whole-mount in situ protein localization in plants. Nat Protoc **1:** 98–103

Smith JM, Leslie ME, Robinson SJ, Korasick DA, Zhang T, Backues SK, Cornish PV, Koo AJ, Bednarek SY, Heese A (2014a) Loss of *Arabidopsis thaliana* Dynamin-Related Protein 2B reveals separation of innate immune signaling pathways. PLoS Pathog **10:** e1004578

Smith JM, Salamango DJ, Leslie ME, Collins CA, Heese A (2014b) Sensitivity to Flg22 is modulated by ligand-induced degradation and de novo synthesis of the endogenous flagellin-receptor FLAGELLIN-SENSING2. Plant Physiol **164:** 440–454

Song J, Lee MH, Lee GJ, Yoo CM, Hwang I (2006) *Arabidopsis* EPSIN1 plays an important role in vacuolar trafficking of soluble cargo proteins in plant cells via interactions with clathrin, AP-1, VTI11, and VSR1. Plant Cell **18:** 2258–2274

Teh OK, Shimono Y, Shirakawa M, Fukao Y, Tamura K, Shimada T, Hara-Nishimura I (2013) The AP-1 μ adaptin is required for KNOLLE localization at the cell plate to mediate cytokinesis in Arabidopsis. Plant Cell Physiol **54:** 838–847

Van Damme D, Coutuer S, De Rycke R, Bouget FY, Inzé D, Geelen D (2006) Somatic cytokinesis and pollen maturation in *Arabidopsis* depend on TPLATE, which has domains similar to coat proteins. Plant Cell **18:** 3502–3518

Van Damme D, Gadeyne A, Vanstraelen M, Inzé D, Van Montagu MC, De Jaeger G, Russinova E, Geelen D (2011) Adaptin-like protein TPLATE and clathrin recruitment during plant somatic cytokinesis occurs via two distinct pathways. Proc Natl Acad Sci USA **108:** 615–620

Viotti C, Bubeck J, Stierhof YD, Krebs M, Langhans M, van den Berg W, van Dongen W, Richter S, Geldner N, Takano J, et al (2010) Endocytic and secretory traffic in *Arabidopsis* merge in the trans-Golgi network/early endosome, an independent and highly dynamic organelle. Plant Cell **22:** 1344–1357

Vlot AC, Dempsey DA, Klessig DF (2009) Salicylic acid, a multifaceted hormone to combat disease. Annu Rev Phytopathol **47:** 177–206

Wang C, Yan X, Chen Q, Jiang N, Fu W, Ma B, Liu J, Li C, Bednarek SY, Pan J (2013a) Clathrin light chains regulate clathrin-mediated trafficking, auxin signaling, and development in *Arabidopsis*. Plant Cell **25:** 499–516

Wang JG, Li S, Zhao XY, Zhou LZ, Huang GQ, Feng C, Zhang Y (2013b) HAPLESS13, the Arabidopsis μ1 adaptin, is essential for protein sorting at the trans-Golgi network/early endosome. Plant Physiol **162:** 1897–1910

Xu J, Scheres B (2005) Dissection of *Arabidopsis* ADP-RIBOSYLATION FACTOR 1 function in epidermal cell polarity. Plant Cell **17:** 525–536

Xu T, Dai N, Chen J, Nagawa S, Cao M, Li H, Zhou Z, Chen X, De Rycke R, Rakusová H, et al (2014) Cell surface ABP1-TMK auxin-sensing complex activates ROP GTPase signaling. Science **343:** 1025–1028

Xu T, Wen M, Nagawa S, Fu Y, Chen JG, Wu MJ, Perrot-Rechenmann C, Friml J, Jones AM, Yang Z (2010) Cell surface- and rho GTPase-based auxin signaling controls cellular interdigitation in *Arabidopsis*. Cell **143:** 99–110

Yamaoka S, Shimono Y, Shirakawa M, Fukao Y, Kawase T, Hatsugai N, Tamura K, Shimada T, Hara-Nishimura I (2013) Identification and dynamics of *Arabidopsis* adaptor protein-2 complex and its involvement in floral organ development. Plant Cell **25:** 2958–2969

Yu Q, Zhang Y, Wang J, Yan X, Wang C, Xu J, Pan J (2016) Clathrin-mediated auxin efflux and maxima regulate hypocotyl hook formation and light-stimulated hook opening in *Arabidopsis*. Mol Plant **9:** 101–112

Zhang Y, Persson S, Hirst J, Robinson MS, van Damme D, Sánchez-Rodríguez C (2015) Change your TPLATE, change your fate: plant CME and beyond. Trends Plant Sci **20:** 41–48

Zouhar J, Sauer M (2014) Helping hands for budding prospects: ENTH/ANTH/VHS accessory proteins in endocytosis, vacuolar transport, and secretion. Plant Cell **26:** 4232–4244

Supplemental Data

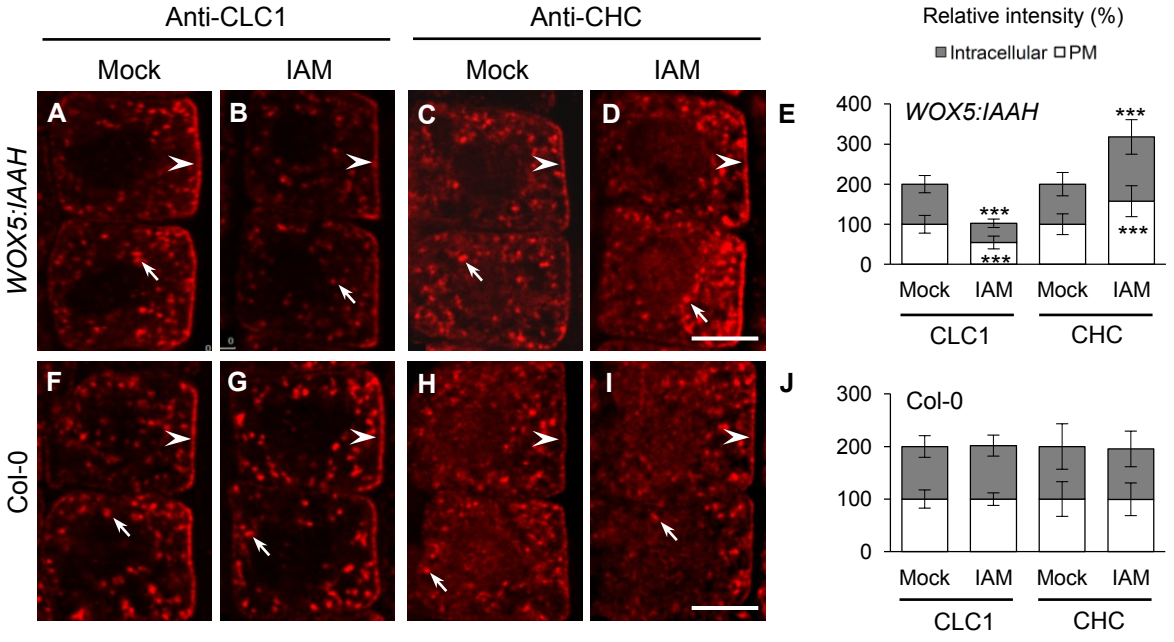

Supplemental Figure S1. Elevation of Endogenous Auxin Levels Affects Clathrin Membrane Association.

A to E, Differential effects of increased endogenous auxin on the membrane association of CLC1 and CHCs in the *WOX5:IAAH* transgenic lines.

F to J, The effect of IAAH substrate, IAM, on the membrane association of CLC1 and CHCs in the wild-type seedlings.

E and J, The relative intensities of PM- and intracellular compartments-associated CLC1 and CHCs (E, *n* = 49-55 cells from 8 or 9 roots each; J, *n* = 39-57 cells from 7-9 roots each).

Five-day-old vertical grown seedlings were incubated for 90 min in 0.5× MS liquid medium supplemented with mock (DMSO) and IAM (5 μM), respectively, before IF analysis.

Arrows and arrowheads show intracellular compartments- and PM-associated CLC1 or CHCs, respectively. Shown are means ± SD. Triple asterisks P < 0.0001 (Student's *t* test; compared to the corresponding mock). Scale bars = 7.5 μm.

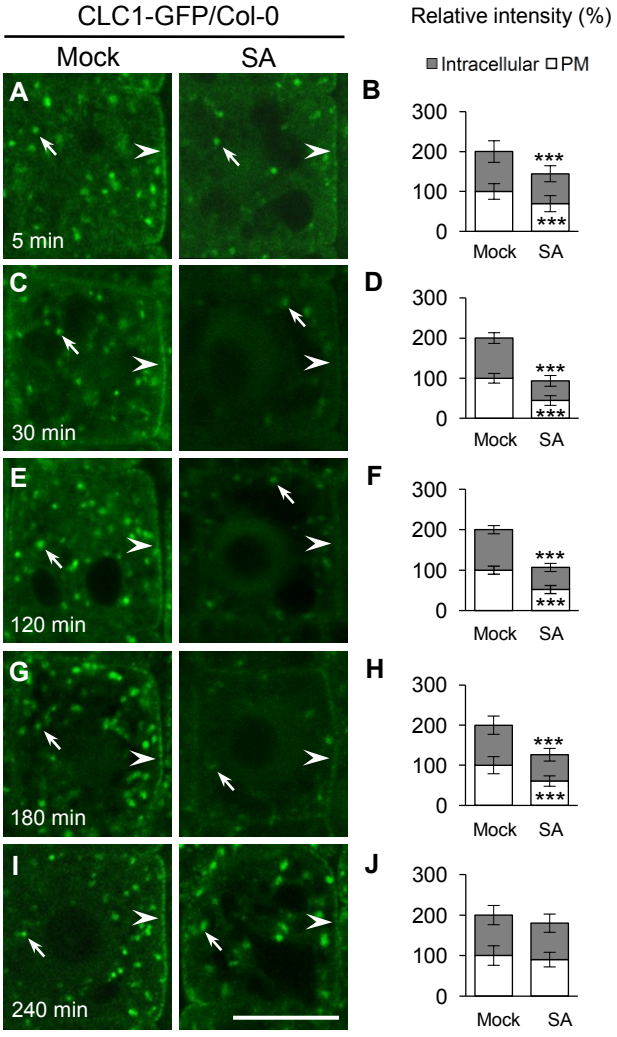

Supplemental Figure S2. Time-Course Analyses of SA Effect on CLC1-GFP Membrane Association.

A to J, The wild-type seedlings expressing CLC1-GFP were treated with mock (DMSO) and SA (25 μM) for different time lengths, respectively.

B, D, F, H, and J, The relative intensity of CLC1-GFP at the PM and intracellular compartments (*n* = 50-65 cells from 8 roots each).

Different time lengths (5, 30, 120, 180, and 240 min) in mock (DMSO) and SA (25 μM) treatments are indicated in the lower-left corners of each panel. Arrows and arrowheads show intracellular compartments- and PM-associated CLC1-GFP, respectively. Shown are means ± SD. Triple asterisks P < 0.0001 (Student's *t* test). Scale bars = 10 μm.

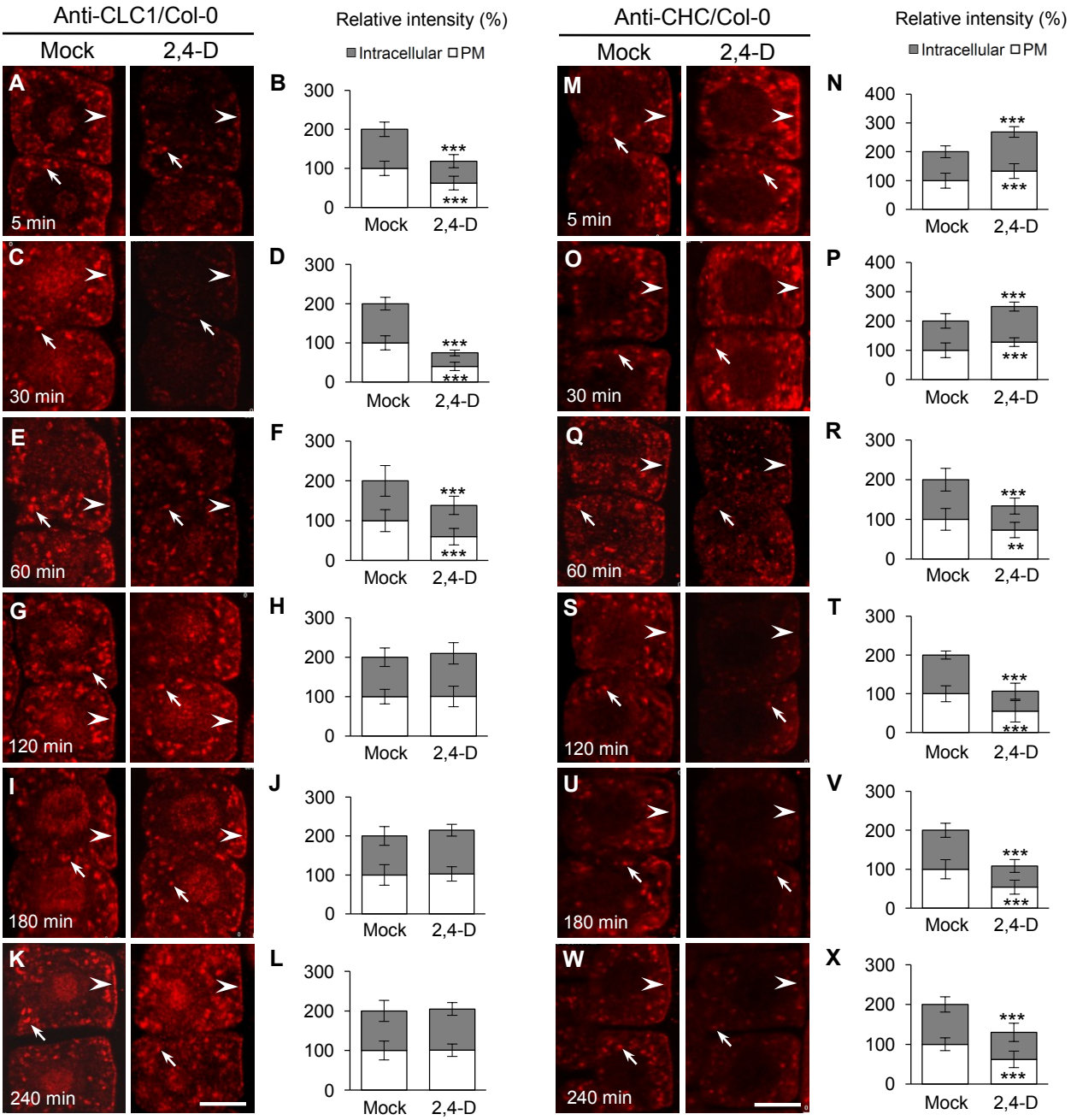

Supplemental Figure S3. Kinetic Effects of Auxin on the Membrane Association of Clathrin.

A to L, Auxin effect on PM- and intracellular compartments-associated CLC1 in the wild type.

M to X, Auxin effect on PM- and intracellular compartments-associated CHC in the wild type.

B, D, F, H, J, and L, The relative intensity of CLC1 at the PM and intracellular compartments (*n* = 54-90 cells from 4-6 roots each).

N, P, R, T, V, and X, The relative intensity of CHC at the PM and intracellular compartments (*n* = 40-68 cells from 6-8 roots each).

Different time lengths (5, 30, 60, 120, 180, and 240 min) in mock (DMSO) and 2,4-D (10 μM) treatments are indicated in the lower-left corners of each panel. Arrows and arrowheads show intracellular compartments- and PM-associated CLC1 or CHC, respectively. Shown are means ± SD. Double and triple asterisks P < 0.001 and 0.0001, respectively (Student's *t* test). Scale bars = 10 μm.

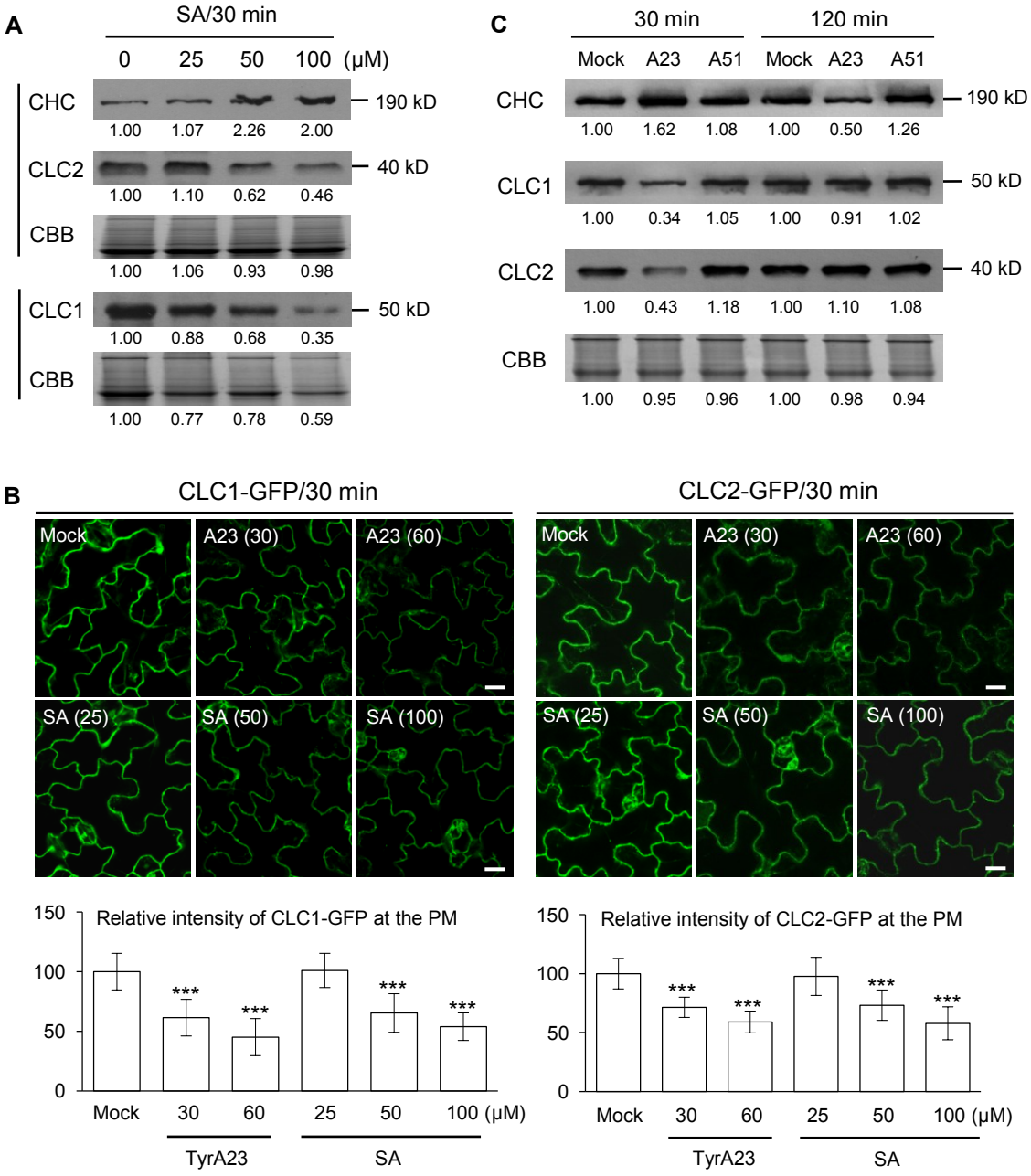

Supplemental Figure S4. Immunoblot and Live-Cell Imaging Analyses of Clathrin Membrane Association.

A and C, Immunoblot analysis of the effects of SA (A) and TyrA23 (C) on the membrane association of CLC1/2 and CHC. Five-day-old seedlings grown in 0.5× MS liquid medium under constant light were treated with different SA concentrations (0, 25, 50, and 100 μM) for 30 min (A), TyrA23 (A23; 0 and 30 μM), and TyrA51 (A51; 0 and 30 μM) for 30 min and 120 min (C), respectively. The microsomal membrane fractions were extracted from the whole seedlings. CBB is Coomassie Brilliant Blue R250 and used as a total protein loading control. Numbers at the bottom of each panel indicate band intensities of CHC and CLC1/2 relative to CBB loading controls, normalized to mock controls (1.00). Loading controls were also normalized to their mock controls.

B, Live-cell microscopy analysis of the effects of TyrA23 and SA on CLC1/2-GFP membrane association in the wild-type cotyledon epidermal cells. The numbers in the brackets show SA and TyrA23 concentrations (μM), while treatment time (30 min) is indicated at the top of the panel. The bottom graphs are quantitative data (n = 77-116 cells from 18 seedlings each). Shown are means ± SD. Triple asterisks $P < 0.0001$ (Student's t test; compared to the mock control). Bars = 20 μm.

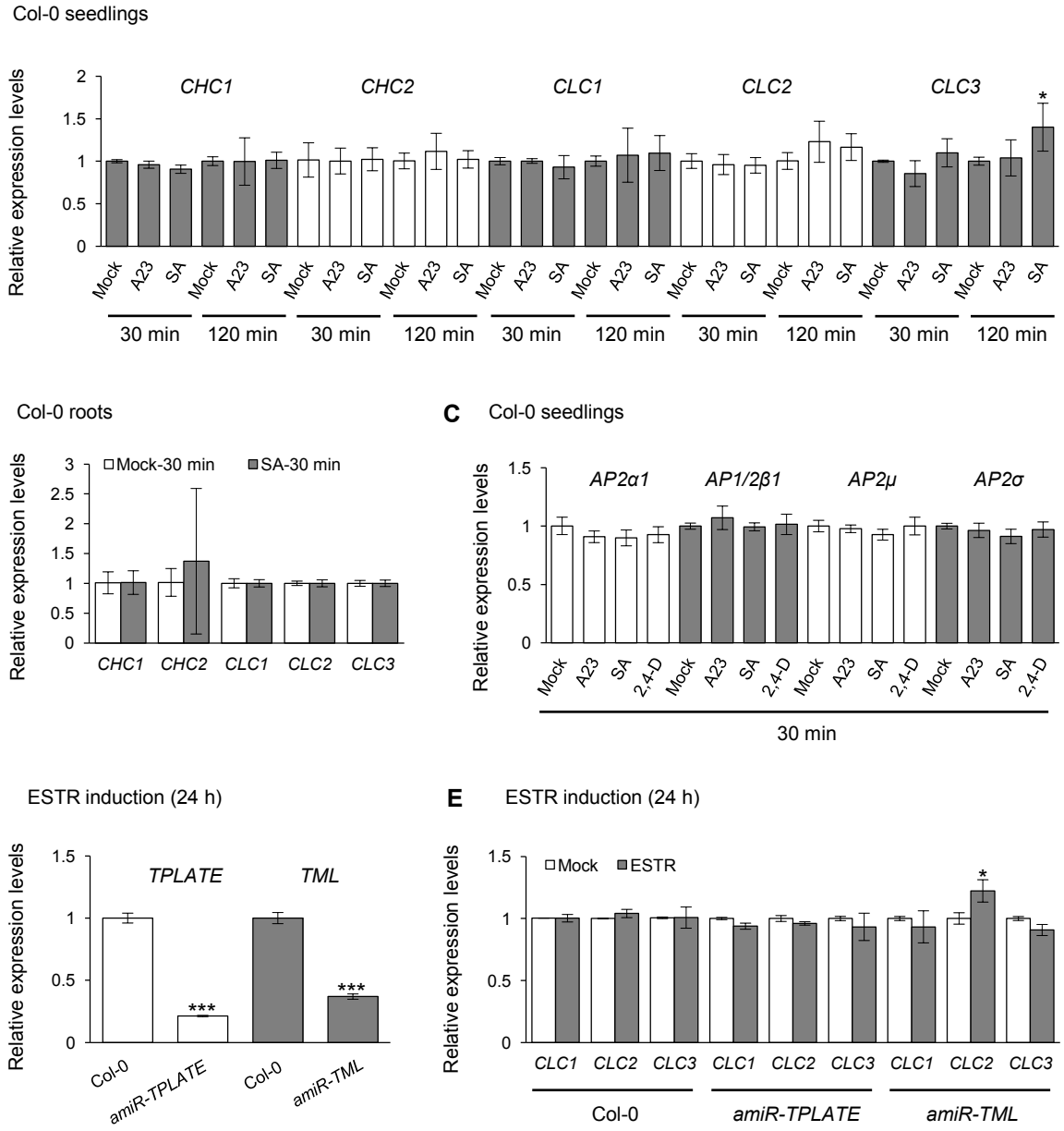

Supplemental Figure S5. qRT-PCR Analysis of Transcriptional Levels of Clathrin and the AP-2/TPC Subunits.

A, Effects of TyrA23 and SA on the transcriptional levels of *CHC1/2* and *CLC1-3* in whole seedlings.

B, SA effect on the transcriptional levels of *CHC1/2* and *CLC1-3* in roots.

C, Effects of TyrA23, SA, and 2,4-D on the transcriptional levels of AP-2 subunits in whole seedlings.

D, Down-regulation of *TPLATE* and *TML* in ESTR-treated *amiR-TPLATE* and *amiR-TML* whole seedlings.

E, Effects of down-regulation of *TPLATE* and *TML* on the transcriptional levels of *CLC1-3* in whole seedlings.

Five-day-old wild-type (Col-0) seedlings (A to C) were treated with mock (DMSO), SA (25 μM), and/or TyrA23 (A23; 30 μM), and/or 2,4-D (10 μM) for 30 min and/or 120 min, respectively, while 4-day-old seedlings (D and E) were treated with ESTR (5 μM) for 24 h. For each gene, the transcription levels in the treatments were presented as a percentage of the corresponding mock or wild-type control. Shown are means ± SD. Single and triple asterisks indicate P < 0.05 and 0.001, respectively (Student's *t* test; compared with the corresponding mock or wild-type control).

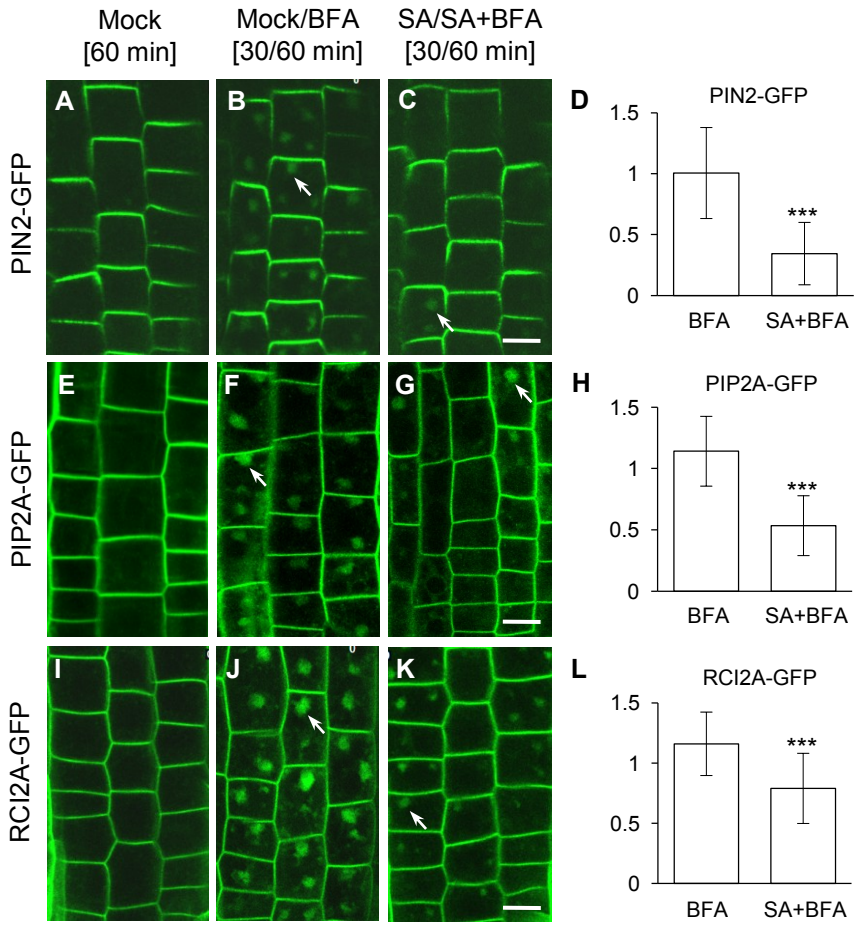

Supplemental Figure S6. Effects of Low Concentrations of SA on Internalization of PM Proteins.

A to L, Five-day-old seedlings expressing PIN2-GFP (A to D), PIP2A-GFP (E to H), RCI2A-GFP (I to L) were pretreated with mock (DMSO) and SA (25 μM) for 30 min followed by washout with mock (DMSO), BFA (50 μM), and SA plus BFA for 60 min, respectively.

D, H, and L, The average number of GFP-labeled BFA bodies (n = 373-522 cells from 14-16 roots each). Arrows show GFP-labeled BFA bodies. Shown are means ± SD. Triple asterisks $P < 0.0001$ (Student's t test). Scale bars = 10 μm.

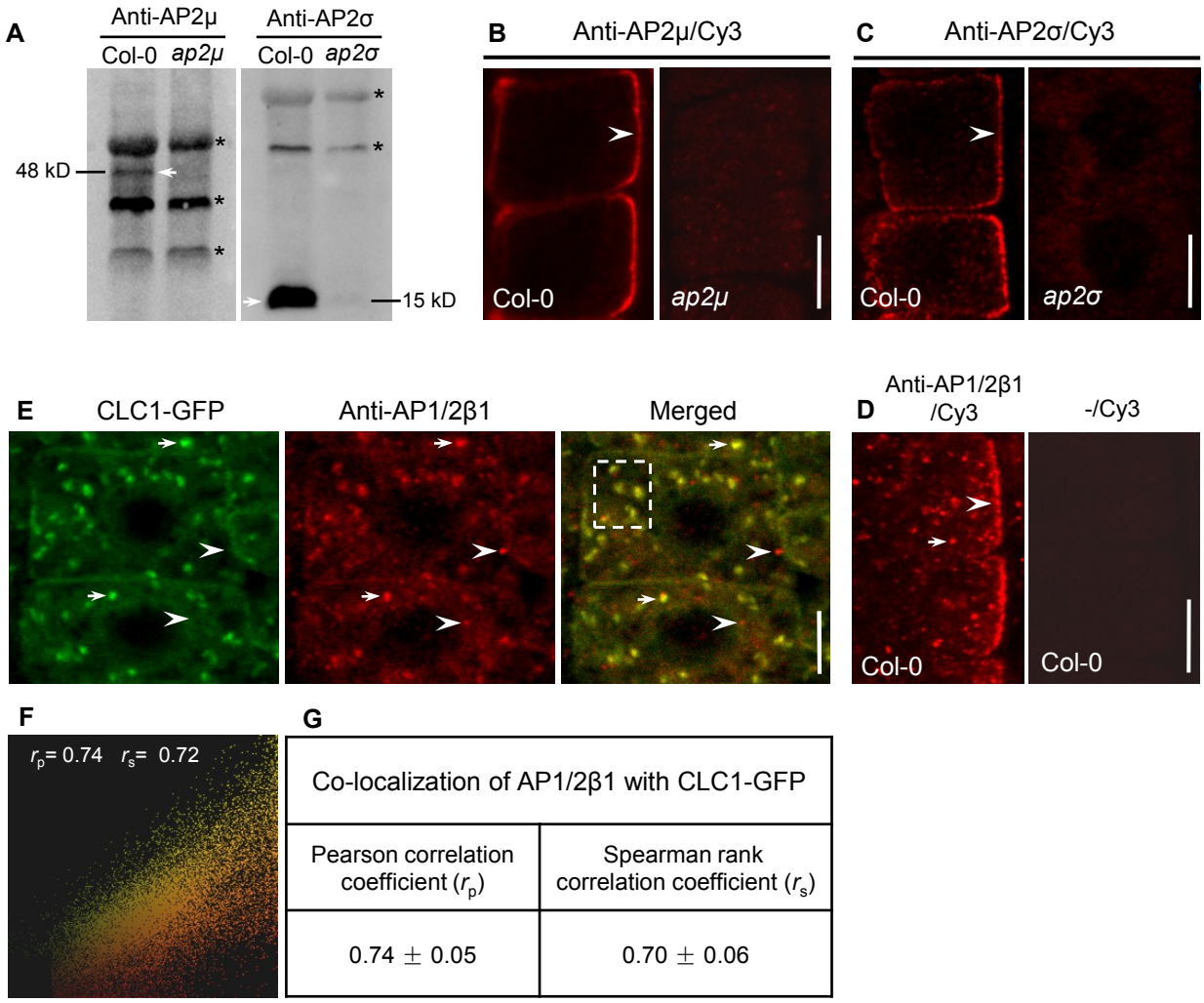

Co-localization of AP1/2β1 with CLC1-GFP	
Pearson correlation coefficient (r_p)	Spearman rank correlation coefficient (r_s)
0.74 ± 0.05	0.70 ± 0.06

Supplemental Figure S7. Immunoblot and IF Analyses of the AP-2 Antibodies.

A to C, Immunodetection of endogenous AP2μ and AP2σ in the wild type, *ap2μ*, and *ap2σ*. A, Immunoblot analysis of total protein extracts from leaf tissues using anti-AP2μ and anti-AP2σ antibodies. B and C, IF analysis in root cells with affinity-purified anti-AP2μ and anti-AP2σ primary antibodies and Cy3-labeled anti-rabbit secondary antibodies, respectively.

D, Indirect immunodetection of AP1/2β1 in the wild-type root cells using affinity-purified anti-AP1/2β1 primary antibodies. Antibody binding was visualized using Cy3-labeled anti-rabbit secondary antibodies (left panel), while control immunolabeling with the Cy3-labeled second antibodies in the absence of primary antibodies (-/Cy3; right panel).

E to G, IF analysis of intracellular co-localization of AP1/2β1 with clathrin. E, Representative images for AP1/2β1 and CLC1-GFP intracellular localization in the root cells. F, A scatter-plot image from (E) shows partial co-localization of AP1/2β1 with CLC1-GFP, quantified by the linear Pearson correlation coefficient (r_p) and the nonlinear Spearman rank correlation coefficient (r_s) indicated in the image. r = 1.0 means complete co-localization of two fluorescent signals. G, Average levels of r_p and r_s from five independent confocal images.

Arrows show specific bands of AP2μ and AP2σ (A) or AP1/2β1 localization at the intracellular compartments (D) or its co-localization with CLC1-GFP (E). Arrowheads show PM-associated AP2μ and AP2σ (B and C) or AP1/2β1 localization at the undefined intracellular compartments (D). Asterisks (A) denote nonspecific polypeptide bands unrelated to AP2μ and AP2σ that crossreact with the anti-AP2μ and -AP2σ antibodies. Shown are means ± SD. Scale bars = 10 μm (B, C, and D), 5 μm (E).

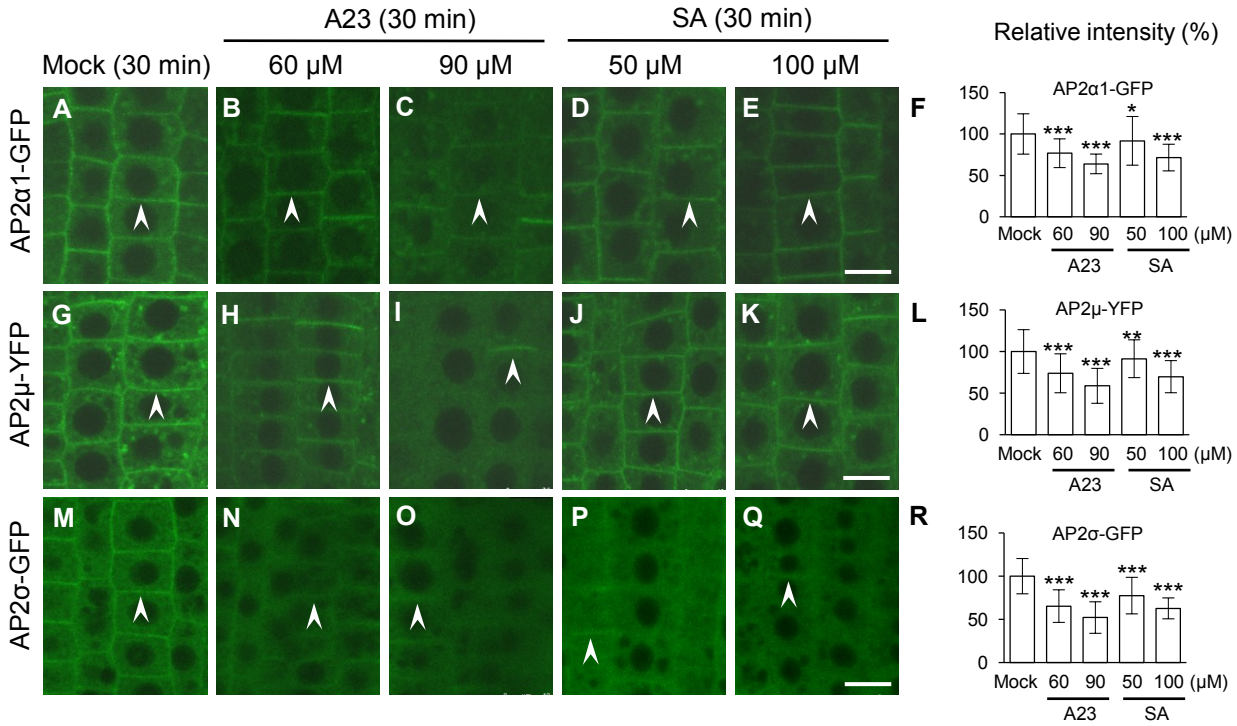

Supplemental Figure S8. Effects of High Concentrations of TyrA23 and SA on the PM Association of AP-2 Subunits.

A to R, Treatments with TyrA23 or SA for 30 min in the seedlings expressing AP2α1-GFP, or AP2μ-YFP (false-colored-green), or AP2σ-GFP.

F, L, and R, The relative intensities of PM-associated GFP- or YFP-fused AP-2 subunits (*n* = 128-156 cells from 8 roots each).

Treatments with mock (DMSO), TyrA23 (A23; 60 and 90 μM), and SA (50 and 100 μM) and duration time (30 min) are indicated at the top of the panels. Arrowheads show PM-associated GFP- or YFP-fused AP-2 subunits. Shown are means ± SD. Single, double, triple asterisks indicate P < 0.05, 0.001, and 0.0001, respectively (Student's *t* test; compared with the mock control). Scale bars = 10 μm.

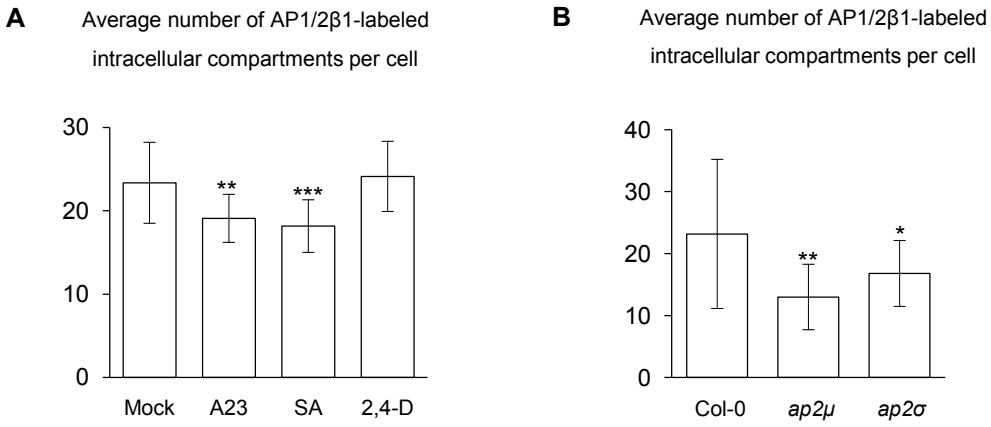

Supplemental Figure S9. Quantification Analysis of AP1/2β1 Intracellular Signals in Figure 4 and Figure 5.

A, The average number of AP1/2β1-labeled intracellular compartments (corresponding to Figure 4, I; *n* = 20-30 cells from 3 or 4 seedlings each)

B, The average number of AP1/2β1-labeled intracellular compartments (corresponding to Figure 5; A and B; G and H; *n* = 42-63 cells from 4 or 5 seedlings each).

Shown are means ± SD. Single, double, and triple asterisks indicate P < 0.05, 0.01 (B) or 0.001 (A), and 0.0001, respectively (Student's *t* test; compared with the mock control or the wild type).

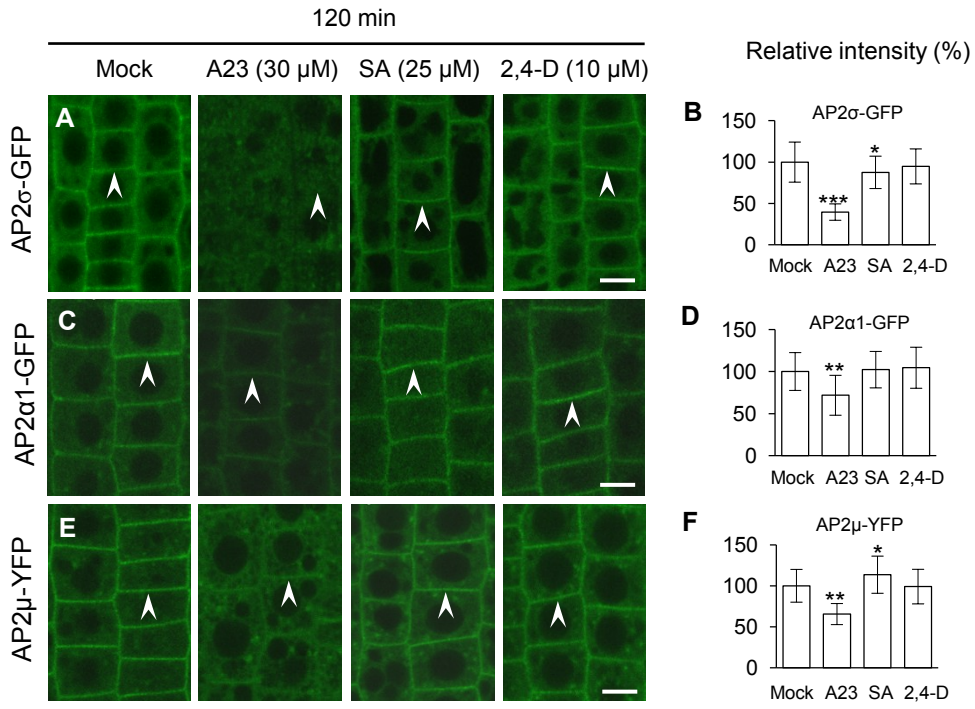

Supplemental Figure S10. Impacts of CME Effectors/Inhibitor on the PM Association of AP-2 Subunits in Extended Treatment.

A to F, Extended treatments (120 min) with CME effectors in the seedling expressing AP2σ-GFP or AP2α1-GFP or AP2μ-YFP (false-colored-green).

B, D, and F, The relative intensities of PM-associated GFP- or YFP-fused AP-2 subunits (*n* = 160-250 cells from 8-12 roots each).

Treatments with mock (DMSO), TyrA23 (A23; 30 μM), SA (25 μM), and 2,4-D (10 μM) and duration time are indicated at the top of the panel, respectively. Arrowheads show PM-associated GFP- or YFP-fused AP-2 subunits. Shown are means ± SD. Single, double, triple asterisks indicate P < 0.05, 0.001, and 0.0001, respectively (Student's *t* test; compared with the mock control). Scale bars = 10 μm.

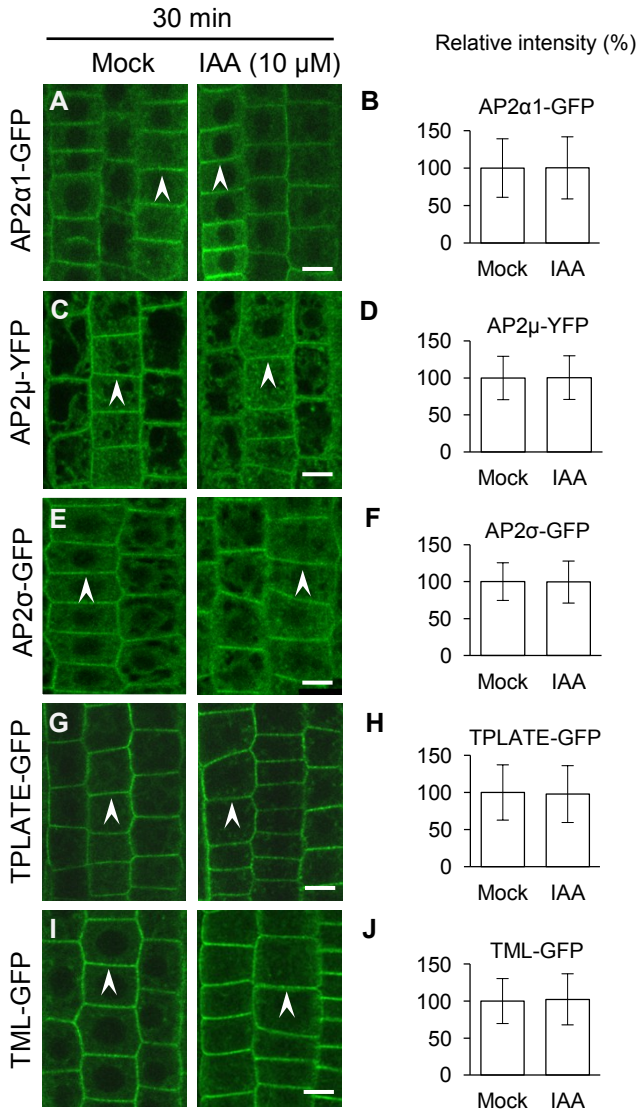

Supplemental Figure S11. Exogenous IAA Effect on the PM Association of the AP-2 and TPC Subunits.

A to F, The effect of IAA treatment on the PM association of AP2α1-GFP (A and B), AP2μ-YFP (C and D), and AP2σ-GFP (E and F).

G to J, The effect of IAA treatment on the PM association of TPLATE-GFP (G and H) and TML-GFP (I and J).

B, D, and F, The relative intensities of PM-associated GFP- or YFP-fused AP-2 subunits (n = 472-817 cells from 18-20 roots each).

H and J, The relative intensities of PM-associated GFP-fused TPC subunits (n = 537-603 cells from 15 roots each).

Arrowheads show PM-associated GFP- or YFP-fused AP-2 or TPC subunits. Scale bars = 10 μm.

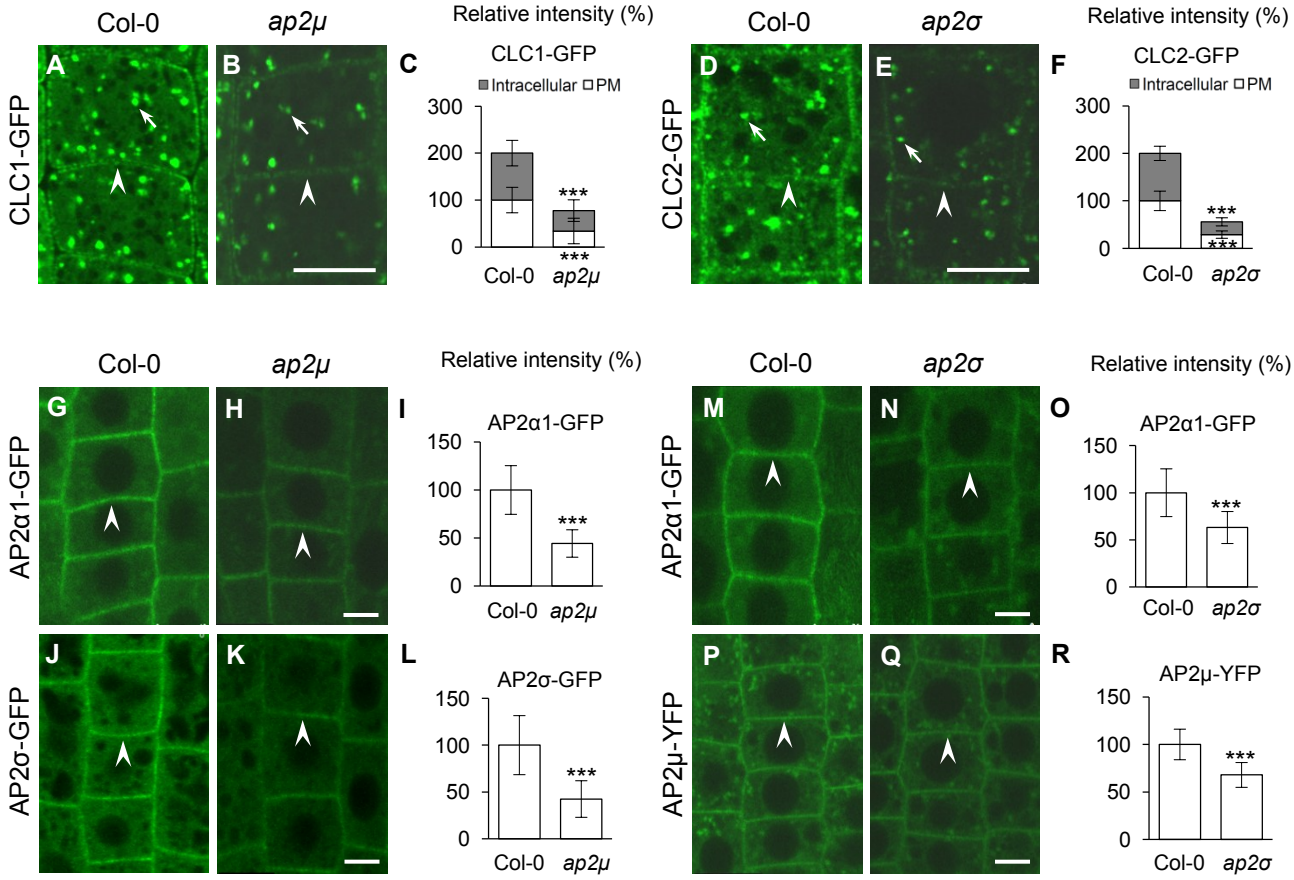

Supplemental Figure S12. Membrane Association of Clathrin and AP-2 Subunits in *ap2σ* and *ap2μ*.

A to F, PM- and intracellular compartments-associated CLC1/2-GFP in the wild-type, *ap2μ*, and *ap2σ* root cells.

G to L, PM-associated AP2α1-GFP and AP2σ-GFP in the wild-type and *ap2μ* root cells.

M to R, PM-associated AP2α1-GFP and AP2μ-YFP in the wild-type and *ap2σ* root cells.

C and F, The relative intensities of CLC1/2-GFP at the PM and intracellular compartments (*n* = 48-93 cells from 4 roots each).

I, L, O, and R, The relative intensities of PM-associated GFP- or YFP-fused AP-2 subunits at the PM (*n* = 145-265 cells from 8 roots each; the quantitative data were summarized in Table 1).

Arrows show PM-associated GFP-fused CLC1/2 subunits, whereas arrowheads show intracellular compartments-associated CLC1/2-GFP or PM-associated fluorescently tagged AP-2 subunits. Shown are means ± SD. Triple asterisks indicate P < 0.0001 (Student's *t* test). Scale bars = 10 μm.

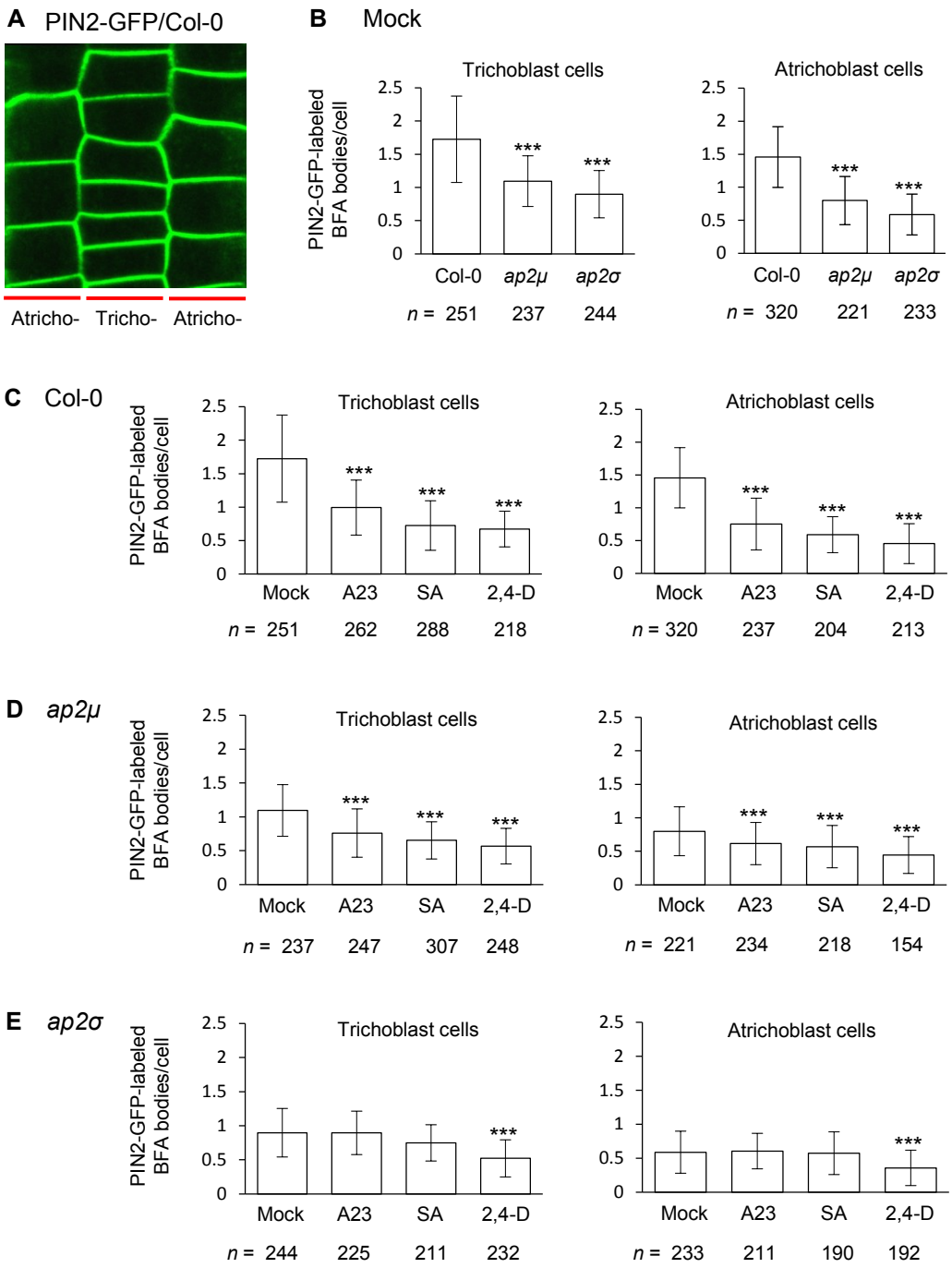

Supplemental Figure S13. Quantification Analysis of PIN2 Endoctyosis in Trichoblast and Atrichoblast Cells in Figure 6.

A, A representative confocal image showing trichoblast and atrichoblast cells of the root expressing PIN2-GFP.

B, The effect of loss of AP2μ or AP2σ on PIN2-GFP internalization in trichoblast and atrichoblast cells treated with mock (corresponding to Fig. 6, B, H, N).

C to E, Impacts of CME effectors/inhibitor on PIN2-GFP internalization in trichoblast and atrichoblast cells of the wild type (C; corresponding to Fig. 5, B to E), *ap2μ* (D; corresponding to Fig. 5, H to K), and *ap2σ* (E; corresponding to Fig. 6, N to Q). Mock controls in (C to E) are identical with those in (B), respectively.

Shown are means ± SD. Triple asterisks indicate P < 0.0001 (Student's *t* test; compared with the corresponding wild-type or mock control). *n*, the total number of examined cells from 11-15 seedlings as indicated at the bottom of graphs.

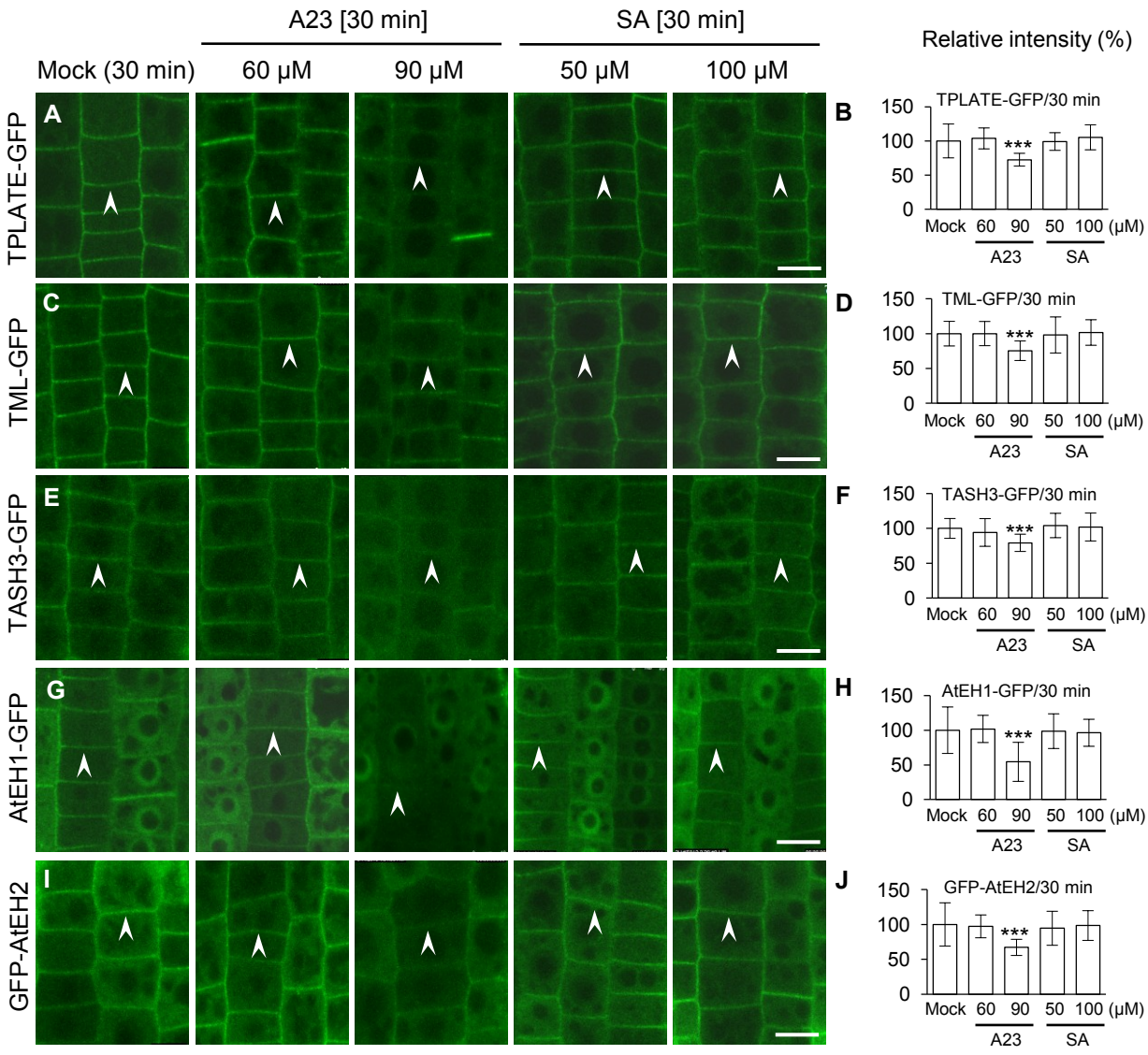

Supplemental Figure S14. Effects of High Concentrations of TyrA23 and SA on the PM Association of the TPC Subunits.

A to J, Treatments with TyrA23 or SA for 30 min in the seedlings expressing GFP-fused TPC subunits.

B, D, F, H, and J, The relative intensities of PM-associated GFP-fused TPC subunits (*n* = 48-120 cells from 4 roots each).

Treatments with mock (DMSO), TyrA23 (A23; 60 and 90 μM), and SA (50 and 100 μM) and duration time are indicated at the top of the panels. Arrowheads show PM-associated GFP-fused TPC subunits. Shown are means ± SD. Triple asterisks indicate P < 0.0001, respectively (Student's *t* test; compared with the mock control). Scale bars = 10 μm.

Supplemental Table S1. Frequency Distribution for the Ratios of Membrane-Associated CLC1 at the Both Sides of Roots.

Frequency Distribution for the Ratios of Membrane-Associated CLC1 (%)				
Ratio[a]	Vertically grown roots[b]		Gravistimulated roots[b]	
	PM	Intracellular	PM	Intracellular
< 0.8	0 (0/37) [c]	0 (0/37)	48.8 (21/43)	53.5 (23/43)
0.8-1.2	94.6 (35/37)	94.6 (35/37)	37.2 (16/43)	37.2 (16/43)
> 1.2	5.4 (2/37)	5.4 (2/37)	14 (6/43)	9.3 (4/43)

[a]The ratios of PM- and intracellular compartments-associated CLC1 signal intensities at the right/left or the bottom/top sides of the root epidermis were artificially classified into three types of the levels: (1) the ratios of < 0.8 indicate reduced signal intensity at the right or bottom side; (2) the ratios of 0.8-1.2 indicate similar signal distribution at the both sides; (3) the ratios of > 1.2 indicate increased signal intensity at the right or bottom side.

[b]The vertically grown seedlings were treated for 2 h with or without gravistimulation.

[c]The fractional number in the brackets denotes that the number of roots with one of three types of the ratios was divided by the total number of examined roots, whereas the number before the brackets is a percentage (%).

Supplemental Table S2. Summary of Effects of Loss of AP2μ or AP2σ on the PM Association of Other AP-2 Subunits.

ap-2 mutants	Reduction (%) in PM-associated levels of the AP-2 subunits			
	AP2α1-GFP	AP1/2β1	AP2μ-YFP /AP2μ	AP2σ-GFP /AP2σ
ap2μ	56% (44.3±14.2***)	49% (51.0±23.9***)	ND	57% (42.5±19.5***) /41% (59.4±31.7***)
ap2σ	37% (63.1±17.0***)	27% (73.4±34.8***)	32% (67.9±13.0***) /37% (63.4±31.7***)	ND

Summary of quantitative data from Fig. 5 and Supplemental Fig. S12. Reduction levels were calculated as100% - % of the wild type. Data (% of the wild type ± SD) in brackets present the PM-associated levels of the AP-2 subunits in *ap2μ* or *ap2σ*. Student's *t* test (***P < 0.0001). ND, not determined. Numbers of roots and cells examined are indicated in the figure legends.

Supplemental Table S3. PCR Primer Sequences for qRT-PCR and Genotyping.

Genes/mutants	Primers	Sequences
AP2α1	*qAP2α1*-F	ACGGATCCCAGCAACCTTAA
	qAP2α1-R	TGCCATTTCCGGAAGAGCTA
AP1/2β1	*qAP1/2β1*-F	CCGGTTGATAGTGCAGCTTC
	qAP1/2β1-R	CTTGAAGCTGGGACGACAAC
AP2μ	*qAP2μ*-F	AATTCCAGTGCCAAAACAAACA
	qAP2μ-R	GCGCGACCAGTTGTCACTT
AP2σ	*qAP2σ*-F	TCCGAGAAACACAAAGTCGA
	qAP2σ-R	GTCGGTTATATCCACGCACAC
UBIQUITIN 7	*qUBI7*-F	CTTCGTCAAAACCCTCACCGGCAAAA
	qUBI7-R	GAGAAGACCACCCCTAAGAGCAAGA
TPLATE	*qTPLATE*-F	CAGGCAGCAGTGCTCCAAG
	qTPLATE-R	CGAAGAAACCACACACAACAAAAG
TML	*qTML*-F	TCGGGATCATGTCGTGTTTA
	qTML-R	AGCAAAATGTCGGATCCATT
ACTIN 2	*qACTIN2*-F	TTGACTACGAGCAGGAGATGG
	qACTIN2-R	AC ACGAGGGCTGGAACAAG
ap-2 mutants		
ap2μ (SALK_083693C)	*ap2μ* -F	AGCTTCTCCTTTTCTTCACCG
	ap2μ -R	TTCATTAAAACCTTCCCCGTC
ap2σ (SALK_141555)	*ap2σ*-F	GATATTGGACCATTTCTTCAGC
	ap2σ-R	TTATCAGTGGAGGACAAAGAAGG
SALK_LBb1		GCGTGGACCGCTTGCTGCAACT

Supplemental Table S4. Information for the AP-2 Antibodies.

Name of antibodies (anti-rabbit)	**Peptide location**	**Sequences**
AP1/2β1	768-779	CFQNMSAGPPSSL
AP2μ	260-274	TRFNSEKTVSFVPPDC
AP2σ	131-142	CIIERMSELEKLQ